PHYSICAL REVIEW D **81,** 074003 (2010)

Anomalous quartic $WW\gamma\gamma$, $ZZ\gamma\gamma$, and trilinear $WW\gamma$ couplings in two-photon processes at high luminosity at the LHC

E. Chapon* and C. Royon†

CEA/IRFU/Service de Physique des Particules, CEA/Saclay, 91191 Gif-sur-Yvette Cedex, France

O. Kepka‡

CEA/IRFU/Service de Physique des Particules, CEA/Saclay, 91191 Gif-sur-Yvette Cedex, France and Center for Particle Physics, Institute of Physics, Academy of Science, Prague, Czech Republic

(Received 19 January 2010; published 5 April 2010)

We study the W/Z pair production via two-photon exchange at the LHC and give the sensitivities on trilinear and quartic gauge anomalous couplings between photons and W/Z bosons for an integrated luminosity of 30 and 200 fb^{-1}. For simplicity and to obtain lower backgrounds, only the leptonic decays of the electroweak bosons are considered.

DOI: 10.1103/PhysRevD.81.074003 PACS numbers: 13.85.Hd, 12.60.Cn

In the standard model (SM) of particle physics, the couplings of fermions and gauge bosons are constrained by the gauge symmetries of the Lagrangian. The measurement of W and Z boson pair productions via the exchange of two photons allows to provide directly stringent tests of one of the most important and least understood mechanism in particle physics, namely, the electroweak symmetry breaking [1]. The non-Abelian gauge nature of the SM predicts the existence of quartic couplings $WW\gamma\gamma$ between the W bosons and the photons, which can be probed directly at the Large Hadron Collider (LHC) at CERN. The quartic coupling $ZZ\gamma\gamma$ is not present in the SM.

The quartic couplings test more generally new physics, which couples to electroweak bosons. Exchange of heavy particles beyond the SM might manifest itself as a modification of the quartic couplings appearing in contact interactions [2]. It is also worth noticing that in the limit of infinite Higgs masses, or in Higgs-less models [2], new structures not present in the tree-level Lagrangian appear in the quartic W coupling. For example, if the electroweak breaking mechanism does not manifest itself in the discovery of the Higgs boson at the LHC or supersymmetry, the presence of anomalous couplings might be the first evidence of new physics in the electroweak sector of the SM.

Two-photon physics is thus a significant enhancement of the LHC physics program [3]. It allows to study the standard model in a unique way at an hadron collider through the exchange of photons. This paper focuses on two applications of the diboson production in two-photon events. First, we propose a measurement of the $pp \to pWWp$ cross section with the use of forward detectors to tag the intact protons, that leave the interaction intact at small angles. Second, we explore the sensitivities to anomalous quartic $WW\gamma\gamma$, $ZZ\gamma\gamma$ (QGC) and triple $WW\gamma$ (TGC) gauge couplings. Benefiting from the enhancement of the cross section when anomalous couplings are considered, the study of QGC sensitivities is performed for two values of integrated luminosity, namely, 30 and 200 fb^{-1} at the LHC at the nominal center-of-mass energy of 14 TeV. To simplify the study and reduce the amount of background, we restrict ourselves to consider only the leptonic decays of the W and Z bosons.

The plan of this paper is as follows: Section I is dedicated to the theoretical framework of the photon induced processes. Section II describes the effective Lagrangians of the anomalous triple and quartic couplings, which we are intending to study. In Sec. III, we discuss the implementation of the two-photon and diffractive processes inside the forward physics Monte Carlo (FPMC) [4], which we use to generate all our signals and backgrounds. In Sec. IV, we describe the methods to extract the diffractive and two-photon events with forward detectors at the LHC. The possibility to observe SM W pair production via two-photon exchange is discussed in Sec. V, and Sec. VI is dedicated to the derivation of the sensitivity to $\gamma\gamma WW$ or $\gamma\gamma ZZ$ anomalous quartic couplings at the LHC. In the last section, we discuss the sensitivity to $WW\gamma$ triple gauge anomalous couplings.

I. TWO-PHOTON EXCHANGE IN THE STANDARD MODEL

In this section, we first describe the theoretical framework of photon induced processes before focusing on the W pair production through the two-photon exchange that we want to measure.

A. Two-photon production cross section

Two-photon production in pp collisions is described in the framework of the equivalent photon approximation [5]. The almost real photons (low photon virtuality $Q^2 = -q^2$) are emitted by the incoming protons producing an object X,

*emilien.chapon@cea.fr
†royon@hep.saclay.cea.fr
‡kepkao@fzu.cz

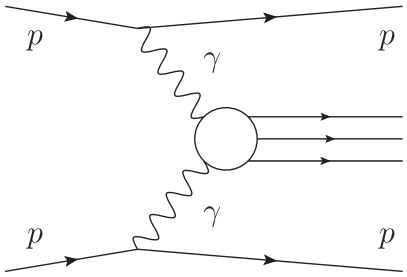

FIG. 1. Sketch diagram showing the two-photon production of a central system. Unaltered protons leave the interaction at very small angles $\lesssim 100$ μrad and the central system is produced alone in the central detector without any proton remnants.

$pp \to pXp$, through two-photon exchange $\gamma\gamma \to X$, see Fig. 1. The photon spectrum of virtuality Q^2 and energy E_γ is proportional to the Sommerfeld fine-structure constant α and reads

$$dN = \frac{\alpha}{\pi}\frac{dE_\gamma}{E_\gamma}\frac{dQ^2}{Q^2}\left[\left(1-\frac{E_\gamma}{E}\right)\left(1-\frac{Q^2_{\min}}{Q^2}\right)F_E + \frac{E_\gamma^2}{2E^2}F_M\right], \tag{1}$$

where E is the energy of the incoming proton of mass m_p, $Q^2_{\min} \equiv m_p^2 E_\gamma^2/[E(E-E_\gamma)]$ the photon minimum virtuality allowed by kinematics, and F_E and F_M are functions of the electric and magnetic form factors. They read in the dipole approximation [5]

$$F_M = G_M^2, \qquad F_E = (4m_p^2 G_E^2 + Q^2 G_M^2)/(4m_p^2 + Q^2),$$
$$G_E^2 = G_M^2/\mu_p^2 = (1 + Q^2/Q_0^2)^{-4}. \tag{2}$$

The magnetic moment of the proton is $\mu_p^2 = 7.78$ and the fitted scale $Q_0^2 = 0.71$ GeV^2. Electromagnetic form factors are steeply falling as a function of Q^2. That is the reason why the two-photon cross section can be factorized into the submatrix element and two-photon fluxes. To obtain the production cross section, the photon fluxes are first integrated over Q^2

$$f(E_\gamma) = \int_{Q^2_{\min}}^{Q^2_{\max}} \frac{dN}{dE_\gamma dQ^2}\, dQ^2 \tag{3}$$

up to a sufficiently large value of $Q^2_{\max} \approx 2$–4 GeV^2. The result can be written as

$$dN(E_\gamma) = \frac{\alpha}{\pi}\frac{dE_\gamma}{E_\gamma}\left(1-\frac{E_\gamma}{E}\right)\left[\varphi\left(\frac{Q^2_{\max}}{Q_0^2}\right) - \varphi\left(\frac{Q^2_{\min}}{Q_0^2}\right)\right], \tag{4}$$

where the function φ definition is

$$\varphi(x) = (1+ay)\left[-\ln(1+x^{-1}) + \sum_{k=1}^{3}\frac{1}{k(1+x)^k}\right] + \frac{(1-b)y}{4x(1+x)^3} + c\left(1+\frac{y}{4}\right)\left[\ln\frac{1+x-b}{1+x} + \sum_{k=1}^{3}\frac{b^k}{k(1+x)^k}\right], \tag{5}$$

where

$$y = \frac{E_\gamma^2}{E(E-E_\gamma)}, \qquad a = \frac{1}{4}(1+\mu_p^2) + \frac{4m_p^2}{Q_0^2} \approx 7.16,$$
$$b = 1 - \frac{4m_p^2}{Q_0^2} \approx -3.96, \qquad c = \frac{\mu_p^2 - 1}{b^4} \approx 0.028. \tag{6}$$

Note that the formula for the Q^2-integrated photon flux was quoted incorrectly several times in the literature. There is a sign error in the original paper in Ref. [5] in the second term of $\varphi(x)$ in Eq. (5). Moreover, in [6] there is another typesetting error leading to wrong second and last terms.

The contribution to the integral above $Q^2_{\max} \approx 2$ GeV^2 is very small. The Q^2-integrated photon flux also falls rapidly as a function of the photon energy E_γ, which implies that the two-photon production is dominant at small masses $W \approx 2\sqrt{E_{\gamma 1}E_{\gamma 2}}$. Integrating the product of the photon fluxes $f(E_{\gamma 1}) \cdot f(E_{\gamma 2}) \cdot dE_{\gamma 1} \cdot dE_{\gamma 2}$ from both protons over the photon energies while keeping the two-photon invariant mass fixed to W, one obtains the two-photon effective luminosity spectrum $dL^{\gamma\gamma}/dW$.

Properties of scattered protons are measured by forward detectors installed hundreds of meters from the interaction point (220 m and 420 m in case of ATLAS, similar in CMS). Scattered proton track segments are reconstructed using several detection planes a few millimeters from the passing beam particles at typical angles smaller than 100 μm. They are used to calculate proton kinematics at the interaction point: the fractional momentum loss of the beam particle $\xi = 1 - |\mathbf{p}|/|\mathbf{p_b}|$, where $\mathbf{p}$ and $\mathbf{p_b}$ are momenta of the scattered and initial beam protons, respectively; the momentum transfer t, and the azimuthal angle ϕ. Since t is very small in two-photon events, ξ is mainly related to the longitudinal momentum loss of the beam protons. Consequently, the photon-photon center of mass energy can be written in terms of the fractional momentum loss and the beam energy as $W = \sqrt{s\xi_1\xi_2}$. The detector coverage of few cm^2 is sufficient to provide ξ acceptance up to ≈ 0.2 and ≈ 0.01 when installed at 220 m and 420 m from the interaction point.

The effective $\gamma\gamma$ luminosity is shown in Fig. 2 as a function of the mass W in full line. The production of heavy objects is particularly interesting at the LHC where new particles could be produced in a very clean environment. The production rate of massive objects is however limited by the photon luminosity at high invariant mass. The integrated two-photon luminosity above $W > W_0$ for

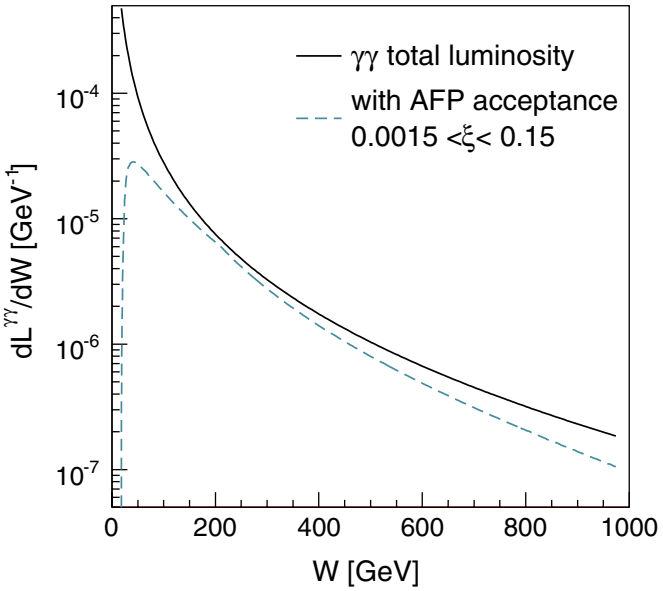

FIG. 2 (color online). Relative effective $\gamma\gamma$ luminosity in pp collisions at 14 TeV as a function of the two-photon invariant mass. The maximal virtualities of the emitted photons are set to $Q^2_{\max} = 2$ GeV^2. The dashed curve shows the photon spectrum within the ATLAS or CMS forward detector acceptance (discussed in Sec. IV).

$W_0 = 23$ GeV, $2 \times m_W \approx 160$ GeV, and 1 TeV is, respectively, 1%, 0.15%, and 0.007% of the luminosity integrated over the whole mass spectrum. The luminosity spectrum was calculated using the upper virtuality bound $Q^2_{\max} = 2$ GeV^2 using numerical integration. The luminosity spectrum within the proposed forward detector acceptance to detect the intact protons $0.0015 < \xi < 0.15$ is also shown in the figure (it is calculated in the limit of low Q^2, thus setting $E_\gamma = \xi E$).

Using the effective relative photon luminosity $dL^{\gamma\gamma}/dW$, the total cross section reads

$$\frac{d\sigma}{d\Omega} = \int \frac{d\sigma_{\gamma\gamma\to X}(W)}{d\Omega} \frac{dL^{\gamma\gamma}}{dW} dW, \tag{7}$$

where $d\sigma_{\gamma\gamma\to X}/d\Omega$ denotes the differential cross section of the subprocess $\gamma\gamma \to X$, dependent on the invariant mass of the two-photon system.

B. W pair production via photon exchanges

The process that we intend to study is the W pair production induced by the exchange of two photons as shown in Fig. 3. It is a pure QED process in which the decay products of the W bosons are measured in the central detector and the scattered protons leave intact in the beam pipe at very small angles, contrary to inelastic collisions. Since there is no proton remnant the process is purely exclusive; only W decay products populate the central detector, and the intact protons can be detected in dedicated detectors located along the beam line far away from the interaction point.

The three-boson $WW\gamma$ and four-boson $WW\gamma\gamma$ interactions,which contribute to the process in the leading order, read

$$\mathcal{L}_{WW\gamma} = -ie(A_\mu W^-_\nu \overleftrightarrow{\partial}^\mu W^{+\nu} + W^-_\mu W^+_\nu \overleftrightarrow{\partial}^\mu A^\nu + W^+_\mu A_\nu \overleftrightarrow{\partial}^\mu W^{-\nu}), \tag{8}$$

$$\mathcal{L}_{WW\gamma\gamma} = -e^2(W^-_\mu W^{+\mu} A_\nu A^\nu - W^-_\mu A^\mu W^+_\nu A^\nu), \tag{9}$$

where the asymmetric derivative has the form $X\overleftrightarrow{\partial}^\mu Y = X\partial^\mu Y - Y\partial^\mu X$.

The production of Z bosons via two-photon exchange is forbidden in the lowest order perturbation theory because neither the Z boson nor the photon carries an electric or weak charge. On the other hand, the W boson can be produced in pairs. In this case, both the triple gauge $WW\gamma$ (with t- and u-channel exchange) and the quartic gauge $WW\gamma\gamma$ boson interactions must be included as shown in Fig. 3.

In the $\gamma\gamma \to WW$ process, the fundamental property of divergence cancellations in the SM at high energy is effective. A necessary condition for the renormalizibility of the standard model at all orders is the so-called ''tree unitarity'' demanding that the unitarity is only minimally (logarithmically) violated in any fixed order of the pertur-

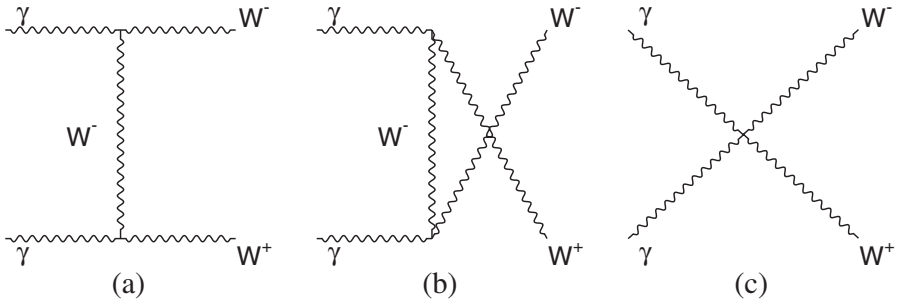

FIG. 3. Feynman diagrams of SM processes that contribute to the $\gamma\gamma \to WW$ scattering amplitude in the lowest order perturbation series with a coupling e^2. The trilinear couplings of strength e are involved in diagrams a) and b) and the direct quartic coupling of strength e^2 in diagram c).

bation series [7,8]. For the binary process of W pair production, in particular, the tree-level unitarity implies that the scattering amplitude $\gamma\gamma \to WW$ should be a constant or vanish in the high-energy limit. In the SM, this condition is indeed satisfied due to the cancellation of divergences stemming from the longitudinal polarizations of W bosons between t-, u-channel and direct quartic diagrams.

The cross section is constant in the high-energy limit. The leading order differential formula for the $\gamma\gamma \to WW$ process is a function of the Mandelstam variables s, t, u and the mass of the vector boson W [9]

$$\frac{d\sigma}{d\Omega} = \frac{3\alpha^2\beta}{2s}\left\{1 - \frac{2s(2s + 3M_W^2)}{3(M_W^2 - t)(M_W^2 - u)} + \frac{2s^2(s^2 + 3M_W^4)}{3(M_W^2 - t)^2(M_W^2 - u)^2}\right\}, \tag{10}$$

where $\beta = \sqrt{1 - 4M_W^2/s}$ is the velocity of the W bosons. For $s \to \infty$ the total cross section is $\sigma_{\text{tot}} = 80.8$ pb.

Measuring the $\gamma\gamma \to WW$ scattering process at the LHC is therefore interesting not only because we can use the hadron-hadron machine as the photon-photon collider with a clean collision environment without beam remnants, but also because it provides a very clear test of the standard model consistency in a rather textbook process.

The cross section of the $pp \to pWWp$ process which proceeds through two-photon exchange is calculated as a convolution (7) of the two-photon luminosity and the total cross section $\gamma\gamma \to WW$ (10). The total two-photon cross section is 95.6 fb.

Since the virtuality of the photon is very close to zero, the electromagnetic coupling appearing in the interaction Lagrangians in Eqs. (8) and (9) is evaluated at the scale $Q^2 = 0$; the electromagnetic fine-structure constant therefore takes the value $\alpha = 1/137$. Note that the above mentioned total cross section is different from the usually presented value of 108 fb (see [10], for example) by about 10%. This is due to the fact that the authors considered the fixed value of the electromagnetic coupling of $1/129$ at the scale of the W mass. In fact, the photon virtuality should be taken as the scale and not the mass of the W. In the Landau gauge, the invariant charge is driven by the self-energy insertion into the photon propagator only (and not by the vertex correction) [11]. In the propagator we have to take the photon virtuality as the scale, which is very small. The total two-photon cross section is therefore $\sigma = 95.6$ fb (this value has to be yet corrected for the survival probability factor, which is expected to be 0.9 at the LHC for exclusive QED processes as discussed bellow).

II. W AND Z PHOTON QUARTIC AND TRILINEAR ANOMALOUS COUPLINGS

The two-photon production of dibosons is very suitable to test the electroweak theory because it allows to probe trilinear and quartic boson couplings. The test is based on deriving the sensitivities with a counting experiment to parameters (coupling strengths) of new auxiliary interaction Lagrangians added to the SM, to simulate low energy effects of some beyond the standard model theories whose typical scales (e.g. the typical new particle masses) are beyond the reach of the LHC energies. In this section, we give the theoretical implementation of quartic and trilinear anomalous couplings between the W or Z boson and the photon in the FPMC generator.

A. Effective quartic anomalous Lagrangian

1. Construction of new quartic anomalous operators

The boson self-interaction in the SM is completely derived from the underlying $\text{SU}(2)_L \times \text{U}_Y(1)$ local symmetry. New vector boson fields are added to the Lagrangian to guarantee the invariance under this symmetry and their self-interactions emerge from the vector boson kinetic terms.

The vector boson masses are, however, more deeply linked with the Higgs field and the vacuum symmetries. The symmetry O(4) of the Higgs potential $V(\Phi) = -\mu^2\Phi^\dagger\Phi + \lambda(\Phi^\dagger\Phi)^2$ is in fact larger than the required $\text{SU}(2) \times \text{U}(1)$. It is known that the symmetry O(4) is locally isomorphic to $\text{O}(4) \simeq \text{SU}(2) \times \text{SU}(2)$. When the symmetry is spontaneously broken and one particular vacuum Φ_U is chosen, the vacuum symmetry is reduced. The vacuum is invariant under SU(2) only. The weak isospin generators $\vec{\tau}/2$ corresponding to the broken symmetry constitute a triplet with respect to the vacuum symmetry subgroup. Very interestingly, this vacuum symmetry controls the value of the ρ parameter

$$\rho = \frac{M_W^2}{M_Z^2\cos^2\theta_W} \tag{11}$$

and is usually called the custodial $\text{SU}(2)_C$ symmetry. The SM value of the parameter is $\rho = 1$, and it was very well confirmed experimentally (taking $m_W = 80.396 \pm 0.025$, $m_Z = 91.1876 \pm 0.021$, and $\sin^2\theta_W = 0.231 \mp 0.00023$ as in [12], we obtain $\rho = 1.011 \pm 0.001$ so it is known with a precision better than 1%). In models with higher Higgs multiplets, ρ can significantly differ from 1. We will assume that this symmetry holds also in more general theories which we are about to parameterize and construct new effective Lagrangian terms in such a way to obey the deeper $\text{SU}(2)_C$ symmetry which is tightly linked with the precisely measured value of the ρ parameter.

The boson self-interactions in the SM (including their kinetic terms) can be conveniently represented by $-\frac{1}{4}W_{\mu\nu} \cdot W^{\mu\nu}$, where the vector

$$\vec{W}_\alpha = \begin{pmatrix} \frac{1}{\sqrt{2}}(W_\alpha^+ + W_\alpha^-) \\ \frac{i}{\sqrt{2}}(W_\alpha^+ - W_\alpha^-) \\ Z_\alpha/\cos\theta_W \end{pmatrix} \tag{12}$$

is a triplet of the custodial $SU(2)_C$ symmetry. The field tensor for W bosons appearing in the product is $\vec{W}_{\mu\nu} = \partial_\mu \vec{W}_\nu - \partial_\nu \vec{W}_\mu + g\vec{W}_\mu \times \vec{W}_\nu$.

In the following, the parameterization of the quartic couplings based on [13] is adopted. We concentrate on the lowest order dimension operators which have the correct Lorentz invariant structure and obey the $SU(2)_C$ custodial symmetry in order to fulfill the stringent experimental bound on the ρ parameter. Also, the $U(1)_Q$ gauge symmetry for those operators which involve photons, is required.

There are only two four-dimension operators:

$$\mathcal{L}_4^0 = \tfrac{1}{4} g_0 g_W (\vec{W}_\mu \cdot \vec{W}^\mu)^2,$$
$$\mathcal{L}_4^C = \tfrac{1}{4} g_C g_W (\vec{W}_\mu \cdot \vec{W}_\nu)(\vec{W}^\mu \cdot \vec{W}^\nu). \quad (13)$$

They are parameterized by the corresponding couplings g_0 and g_C. Using the explicit form of the $SU(2)_C$ triplet we see that these Lagrangians do not involve photons. Clearly, it is not possible to construct any operator of dimension 5 since an even number of Lorentz indices is needed to contract the field indices. Thus the lowest order interaction Lagrangians which involve two photons are dimension-six operators. There are two of them:

$$\mathcal{L}^0 = -\frac{\pi\alpha}{4\Lambda^2} a_0 F_{\alpha\beta} F^{\alpha\beta} (\vec{W}_\mu \cdot \vec{W}^\mu), \quad (14)$$

$$\mathcal{L}^C = -\frac{\pi\alpha}{4\Lambda^2} a_C F_{\alpha\mu} F^{\alpha\nu} (\vec{W}^\mu \cdot \vec{W}^\nu) \quad (15)$$

parameterized with new coupling constants a_0, a_C, and the fine-structure constant $\alpha = e^2/(4\pi)$. The new scale Λ is introduced so that the Lagrangian density has the correct dimension four and is interpreted as the typical mass scale of new physics. Expanding the above formula using the definition of the $SU(2)_C$ triplet and expressing the product

$$\vec{W}_\mu \cdot \vec{W}_\nu = 2\left(W_\mu^+ W_\nu^- + \frac{1}{2\cos^2\theta_W} Z_\mu Z_\nu\right), \quad (16)$$

we arrive at the following expression for the effective quartic Lagrangian

$$\mathcal{L}_6^0 = \frac{-e^2}{8} \frac{a_0^W}{\Lambda^2} F_{\mu\nu} F^{\mu\nu} W^{+\alpha} W^-_\alpha - \frac{e^2}{16\cos^2\theta_W} \frac{a_0^Z}{\Lambda^2} F_{\mu\nu} F^{\mu\nu} Z^\alpha Z_\alpha,$$
$$\mathcal{L}_6^C = \frac{-e^2}{16} \frac{a_C^W}{\Lambda^2} F_{\mu\alpha} F^{\mu\beta} (W^{+\alpha} W^-_\beta + W^{-\alpha} W^+_\beta) - \frac{e^2}{16\cos^2\theta_W} \frac{a_C^Z}{\Lambda^2} F_{\mu\alpha} F^{\mu\beta} Z^\alpha Z_\beta. \quad (17)$$

In the above formula, we allowed the W and Z parts of the Lagrangian to have specific couplings, i.e. $a_0 \to (a_0^W, a_0^Z)$ and similarly $a_C \to (a_C^W, a_C^Z)$. From the structure of $\mathcal{L}_6^0$ in which the indices of photons and W are decoupled, we see that this Lagrangian can be interpreted as the exchange of a neutral scalar particle whose propagator does not have any Lorentz index. Such Lagrangian density conserves C-, P-, and T-parities separately and hence represents the most natural extension of the SM. On the other hand, one may as well construct other dimension-six operators, which violate these symmetries. Such operators are omitted in this work.

The current best experimental 95% C.L. limits on the above anomalous parameters come from the OPAL Collaboration where the quartic couplings were measured in $e^+e^- \to W^+W^-\gamma$, $e^+e^- \to \nu\bar{\nu}\gamma\gamma$ (for $WW\gamma\gamma$ anomalous couplings), and $e^+e^- \to q\bar{q}\gamma\gamma$ (for $ZZ\gamma\gamma$ couplings) at center-of-mass energies up to 209 GeV. The corresponding 95% confidence level limits on the anomalous coupling parameters were found [14]

$$-0.020\ \text{GeV}^{-2} < a_0^W/\Lambda^2 < 0.020\ \text{GeV},^{-2}$$
$$-0.052\ \text{GeV}^{-2} < a_C^W/\Lambda^2 < 0.037\ \text{GeV},^{-2}$$
$$-0.007\ \text{GeV}^{-2} < a_0^Z/\Lambda^2 < 0.023\ \text{GeV},^{-2}$$
$$-0.029\ \text{GeV}^{-2} < a_C^Z/\Lambda^2 < 0.029\ \text{GeV}^{-2}. \quad (18)$$

On the other hand, there has not been any direct constraint on the anomalous quartic couplings reported from the Tevatron so far.

2. Coupling form factors

The WW and ZZ two-photon cross sections rise quickly at high energies when any of the anomalous parameters are nonzero, as illustrated in Fig. 4. As was already mentioned,

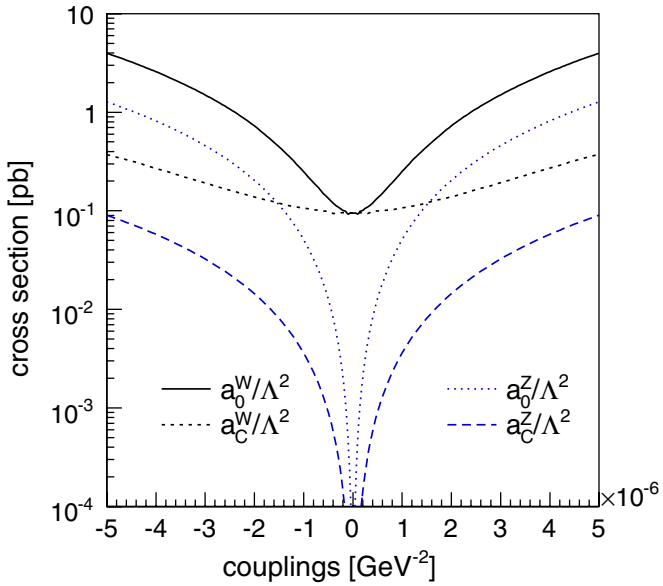

FIG. 4 (color online). Enhancement of the $pp \to pWWp$ and $pp \to pZZp$ cross section at $\sqrt{s} = 14$ TeV with quartic anomalous couplings a_0^W, a_C^W, and a_0^Z, a_C^Z from the SM values 95.6 fb and 0, respectively. The survival probability factor is not included.

the tree-level unitarity uniquely restricts the $WW\gamma\gamma$ coupling to the SM values at asymptotically high energies. This implies that any deviation of the anomalous parameters a_0^W/Λ^2, a_C^W/Λ^2, a_0^Z/Λ^2, a_C^Z/Λ^2 from the SM zero value will eventually violate unitarity. Therefore, the cross section rise have to be regulated by a form factor which vanishes in the high-energy limit to construct a realistic physical model of the beyond the standard model theory. At LEP where the center-of-mass energy was rather low, the wrong high-energy behavior did not violate unitarity; however, it must be reconsidered at the LHC. We therefore modify the couplings introduced in (17) by form factors that have the desired behavior, i.e. they modify the coupling at small energies only slightly but suppress it when the center-of-mass energy $W_{\gamma\gamma}$ increases. The form of the form factor that we consider is

$$a \rightarrow \frac{a}{(1 + W_{\gamma\gamma}^2/\Lambda^2)^n}. \tag{19}$$

The exact form of the form factor is not imposed but rather only conventional and the same holds for the value of the exponent n. Λ^2 corresponds to the scale where new physics should appear and where the new type of production would regularize the divergent high-energy behavior of the Lagrangians (17).

The unitarity of the scattering S matrix imposes a condition on the partial waves amplitudes defined as

$$a_J(\sqrt{s}) = \frac{1}{32}\int_{-1}^{1} d(\cos\theta)\mathcal{A}(\sqrt{s}, \cos\theta, a_0, a_C)P_J(\cos\theta), \tag{20}$$

where $P_J(\cos\theta)$ are the Legendre polynomials depending on the polar angle in the $\gamma\gamma$ center of mass. The unitarity condition of the J scattering amplitude in the $\gamma\gamma \rightarrow WW$ process reads

$$\beta\sum_{\lambda_1,\lambda_2}|a_J(\sqrt{s})|^2 \leq \frac{1}{4}, \tag{21}$$

where $\beta = \sqrt{1 - 4m_W^2/s}$ is the velocity of a W boson in the center-of-mass frame and the λ_1, λ_2 indices denote the W polarization states.

For the anomalous interaction (17), the most restrictive bounds come from the $J = 0$ partial wave, which can be easily understood since Ws with longitudinal polarizations without any spin flip are dominantly produced in this case. For $J = 0$, the unitarity bounds read [15]

$$\frac{1}{N}\left(\frac{\alpha a s}{16}\right)^2\left(1 - \frac{4M_W^2}{s}\right)^{1/2}\left(3 - \frac{s}{M_W^2} + \frac{s^2}{4M_W^4}\right) \leq 1 \quad \text{for } V = W, \tag{22}$$

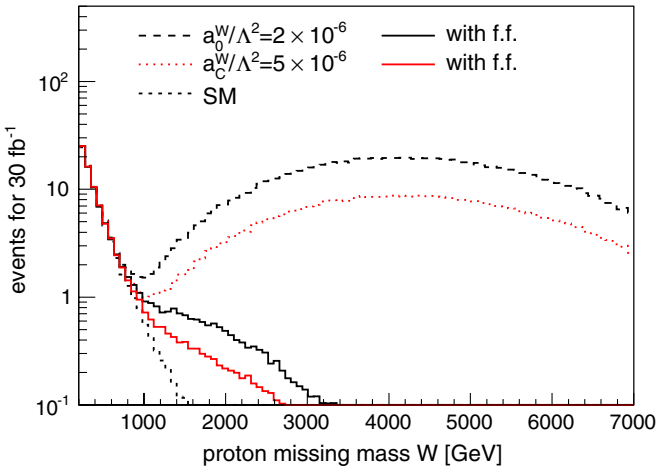

FIG. 5 (color online). Missing mass distribution showing the effect of the form factor (19) on the cross section. The signal due to the anomalous coupling appears for masses $W > 800$ GeV. Both leptons are in the detector acceptance and above $p_T > 10$ GeV.

$$\frac{1}{N}\left(\frac{\alpha a s}{16\cos^2\theta_W}\right)^2\left(1 - \frac{4M_Z^2}{s}\right)^{1/2}\left(3 - \frac{s}{M_Z^2} + \frac{s^2}{4M_Z^4}\right) \leq 1 \quad \text{for } V = Z, \tag{23}$$

where $a = a_0/\Lambda^2$ or a_C/Λ^2 and $N = 1/4(4)$ for a_0/Λ^2 (a_C/Λ^2).

The unitarity violation in $\gamma\gamma \rightarrow WW$ process was also investigated in Ref. [10]. For relevant values of a_0^W, which are to be probed at the LHC using forward detectors, it was found that unitarity is violated around $W_{\gamma\gamma} = 2$ TeV for the form factor exponent $n = 2$. We adopt this type of form factor for the following study, i.e. the form factor

$$a \rightarrow \frac{a}{[1 + (W_{\gamma\gamma}/2\ \text{TeV})^2]^2} \tag{24}$$

is introduced for all quartic couplings $a = a_0^W/\Lambda^2, a_C^W/\Lambda^2, a_0^Z/\Lambda^2, a_C^Z/\Lambda^2$. The suppression of the signal at high mass due to the coupling form factors is shown in Fig. 5 for $a_0^W = 2\times10^{-6}$ and $a_0^C = 5\times10^{-5}$ GeV^{-2}. The unitarity condition (22) for couplings $a_0^W/\Lambda^2 = 10^{-5}$ and 10^{-6} GeV^2 is illustrated in Fig. 6. First, we see that couplings without the form factors violate unitarity already at TeV energies. On the other hand, employing the form factors as described above justifies the nonviolation of the unitarity of events inside the AFP acceptance ($W \lesssim 2$ TeV) if the resulting limits on neutral couplings a_0 are of the order of 10^{-6} GeV^{-2}. For the charged couplings a_C the unitarity condition is less strict due to $N = 4$ in Eqs. (22) and (23).

B. Anomalous triple gauge $WW\gamma$ couplings

In this section, we introduce the effective triple gauge $WW\gamma$ couplings (TGC). The TGC have already been quite

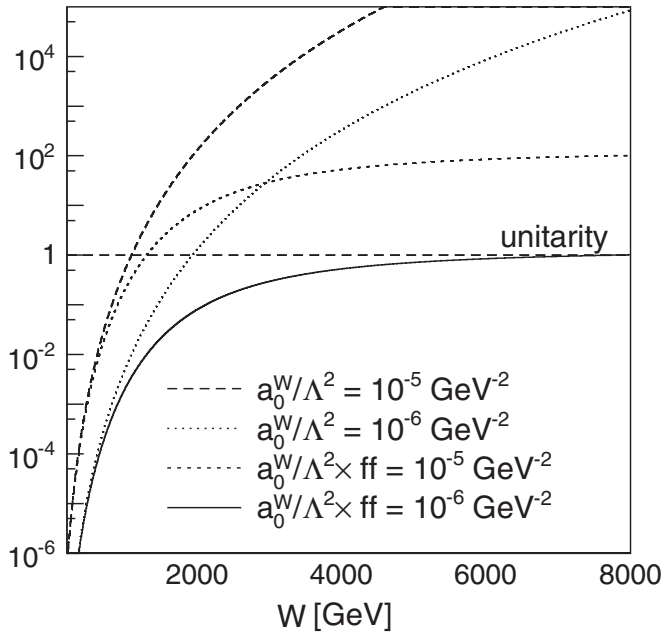

FIG. 6. The unitarity condition (22) for quartic anomalous couplings $a_0^W/\Lambda^2 = 10^{-5}$ and 10^{-6} GeV^2 as a function of two-photon invariant mass. The unitarity is violated above the horizontal line at 1. The form of the form factor (24) is used for the two bottom curves.

well constrained at LEP. Note that the lowest dimensional triple gauge boson operator $ZZ\gamma$ is of dimension six, the effect of this coupling in two-photon events will be the subject of a further study. First, the effective Lagrangians describing the triple gauge couplings are introduced before evaluating the anomalous cross section.

1. Effective triple gauge boson operators

The most general form of an effective Lagrangian $\mathcal{L}_{WW\gamma}$ involving two charged vector bosons W and one neutral vector boson has only seven terms which have the correct Lorentz structure (see [16,17] for details). This is because only seven out of the nine helicity states of the W pair production can be reached with the spin-1 vector boson exchange. The other two states have both W spins pointing in the same direction with an overall spin 2.

Furthermore, only three out of the seven operators preserve the P-, C- and T-discrete symmetries separately. We restrict ourselves to study this subset of operators. They are the following:

$$\mathcal{L}/g_{WW\gamma} = i(W^+_{\mu\nu}W^\mu A^\nu - W_{\mu\nu}W^{+\mu}A^\nu) + i\kappa^\gamma W^+_\mu W_\nu A^{\mu\nu} + i\frac{\lambda^\gamma}{M_W^2} W^+_{\rho\mu}W^{\mu}{}_{\nu}A^{\nu\rho}, \tag{25}$$

where the tensor is $W_{\mu\nu} = \partial_\mu W_\nu - \partial_\nu W_\mu$, $g_{WW\gamma} = e$ is the trilinear coupling in the SM model whose strength is fixed by the charge of the W, and κ^γ and λ^γ are the anomalous parameters, and their values are 1 and 0 in the SM, respectively. They can be related to the magnetic μ_W and electric Q_W moments of the W^+ by

$$\mu_W = \frac{e}{2m_W}(1 + \Delta\kappa^\gamma + \lambda^\gamma), \qquad Q_W = \frac{e}{m_W^2}(\Delta\kappa^\gamma - \lambda^\gamma), \tag{26}$$

where $\Delta\kappa^\gamma \equiv \kappa^\gamma - 1$ describes the deviation of the parameter from the SM value. (it is straightforward to verify that (25) gives the SM trilinear Lagrangian (8) for $\kappa^\gamma = 1$ and $\lambda^\gamma = 0$. Our convention differs from the one in [16] by an overall factor -1).

The current best 95% C.L. limits on anomalous couplings come from the combined fits of all LEP experiments [18].

$$-0.098 < \Delta\kappa^\gamma < 0.101 \qquad -0.044 < \lambda^\gamma < 0.047. \tag{27}$$

The CDF collaboration presented the most stringent constraints on $WW\gamma$ coupling measured at hadron colliders [19]

$$-0.51 < \Delta\kappa^\gamma < 0.51 \qquad -0.12 < \lambda^\gamma < 0.13 \tag{28}$$

analyzing the $W\gamma$ events in proton-antiproton interactions. Even though the LEP results are more precise than the results from the hadron collider, there is always a mixture of γ and Z exchanges present in the process $e^+e^- \to WW$ from which the couplings are extracted. The two-photon WW production at the LHC has the advantage that pure $W-\gamma$ couplings are tested and no SM Z exchange is present.

2. Anomalous cross section

The effect of the two anomalous couplings is different. The total cross section is much more sensitive to the anomalous coupling λ^γ. As shown in Fig. 7, the SM cross section $\sigma_{\rm SM} = 95.6$ fb is a global minimum with respect to the λ^γ parameter. For $\Delta\kappa^\gamma$ the minimum also exists but for large negative values which have already been excluded by experiments. The last term proportional to λ^γ in (25) does not have a dimensionless coupling. With simple dimensional consideration we see that the $\gamma\gamma \to WW$ scattering amplitude which has to be dimensionless will have the form $\sim \frac{W^4}{M_W^4}$ and will therefore be quickly rising as a function of the two-photon mass W. This is seen in Fig. 8 where the cross section is shown as a function of the momentum fraction loss of the proton. $\Delta\kappa^\gamma$ enhances the overall normalization of the distribution (left) whereas λ^γ gives rise to the ξ tail (right) as anticipated.

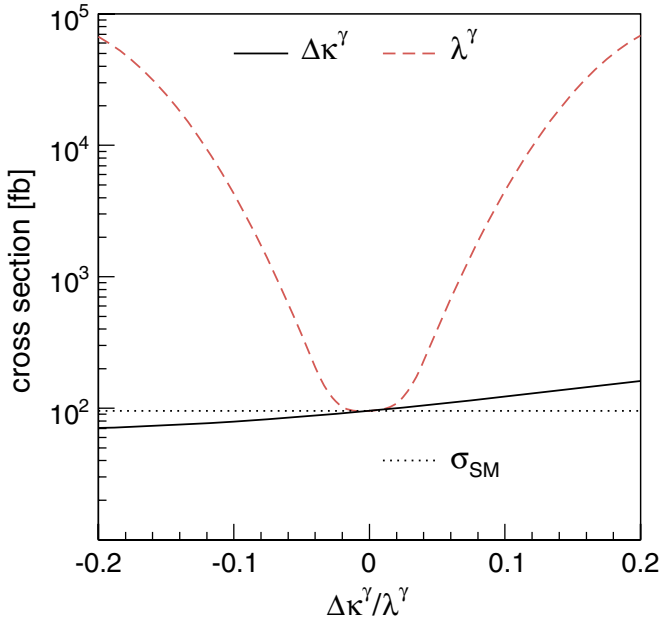

FIG. 7 (color online). Enhancement of the total cross section with the triple-boson anomalous couplings $\Delta\kappa^\gamma$, λ^γ. The rise of the cross section due to λ^γ is well pronounced whereas the dependence on $\Delta\kappa^\gamma$ is modest (the tail for large negative $\Delta\kappa^\gamma$ where cross section increases is not shown).

C. Coupling form factors

The rise of the cross section for anomalous TGC at high energy leads again to the violation of unitarity. The enhancement of the cross section has to be again regulated by appropriate from factors. We apply the same form factors as already mentioned for the quartic couplings (24).

III. THE FORWARD PHYSICS MONTE CARLO

In this section, we briefly describe the FPMC generator [4] used extensively in this paper to produce all signal and background events. FPMC aims to accommodate all relevant models for forward physics which could be studied at the LHC and contains, in particular, the two-photon and double Pomeron exchange processes which are relevant for this study since we focus on events in which both protons are detected. The generation of the forward processes is embedded inside HERWIG [20]. The advantage of the program is that all the processes with leading protons can be studied in the same framework, using the same hadronization model. It is dedicated to generate the following exchanges:

(i) two-photon exchange
(ii) single diffraction
(iii) double Pomeron exchange
(iv) central exclusive production

In FPMC, the diffractive and exclusive processes are implemented by modifying the HERWIG routine for the $e^+e^- \rightarrow (\gamma\gamma) \rightarrow X$ process. In case of the two-photon pp events, as we mentioned in Sec. I, the Weizsäcker-Williams formula describing the photon emission off pointlike electrons is substituted by the Budnev flux [5], which describes properly the coupling of the photon to the proton, taking into account the proton electromagnetic structure.

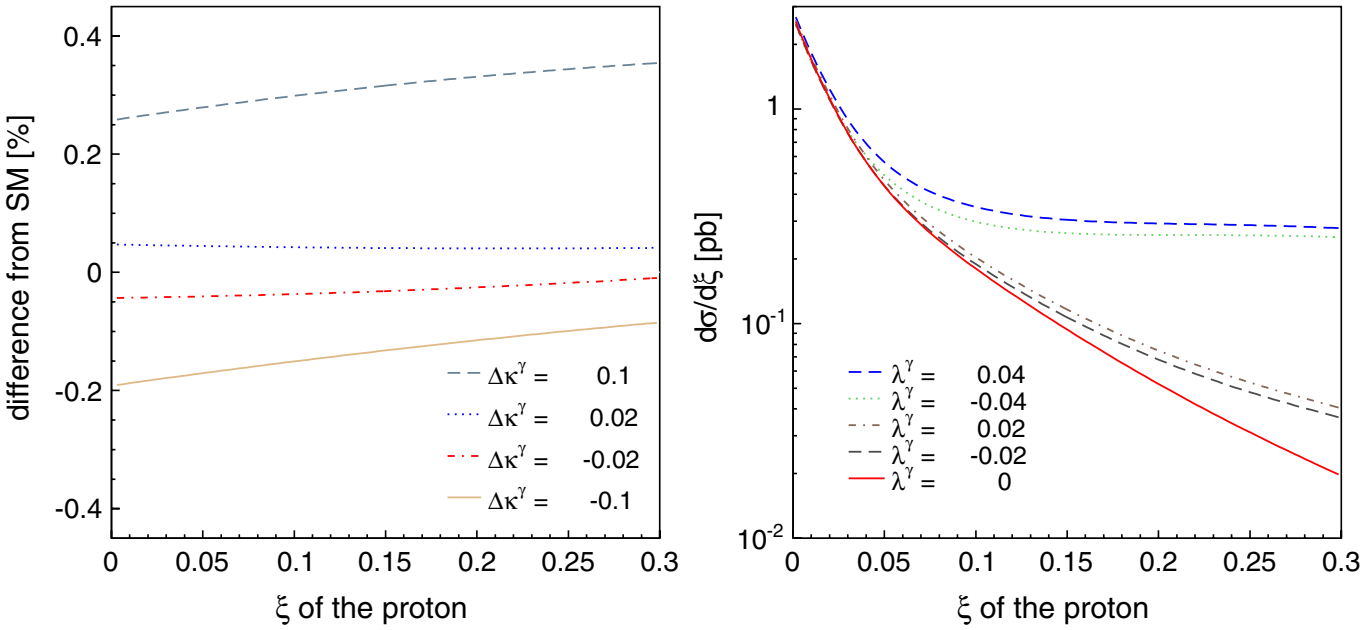

FIG. 8 (color online). ξ dependence of the two-photon WW cross section for different values of $\Delta\kappa^\gamma$ (left) and λ^γ (right) [SM values are 0]. For λ^γ, the cross section is enhanced at high ξ which is at the edge of the forward detector acceptance ($\xi = 0.15$). On the contrary, varying $\Delta\kappa^\gamma$ in the interesting range ($-0.05 < \Delta\kappa^\gamma < 0.05$) changes mainly the normalization and not the shape of the ξ distribution.

The effective Lagrangians parametrizing new interactions of electroweak bosons mentioned explicitly in Eqs. (17) and (25) are functions of six anomalous parameters: $\Delta\kappa^\gamma$, λ^γ for the triple gauge couplings and a_0^W/Λ^2, a_C^W/Λ^2, a_0^Z/Λ^2, a_C^Z/Λ^2 for the quartic ones. The corresponding matrix elements squared were obtained with the COMPHEP program [21] whose output was interfaced with FPMC.

The single diffractive and double Pomeron exchange events are produced in FPMC using the diffractive parton densities measured at HERA [22]. The outcome of the QCD Dokshitzer-Gribov-Lipatov-Altarelli-Parisi [23] fits to the proton diffractive structure functions are the values of the Pomeron and Reggeon trajectories $\alpha_{\mathbb{P}}(t) = \alpha_{\mathbb{P}}(0) + t\alpha'_{\mathbb{P}}$, $\alpha_{\mathbb{R}}(t) = \alpha_{\mathbb{R}}(0) + t\alpha'_{\mathbb{R}}$ governing the corresponding flux energy and t dependences, and the Pomeron parton distribution functions.

In addition, the experimental signature of the two-photon or DPE interaction in which two scattered protons emerge intact in the beam pipe and can be tracked in forward detectors, can be lost by additional soft interactions between the outgoing protons. The survival probabilities for the QED two-photon processes and QCD diffractive and central exclusive processes are therefor introduced and assumed to be 0.9 and 0.03 [24].

Technically, in FPMC, for processes in which the partonic structure of the Pomeron is probed, the existing HERWIG matrix elements of nondiffractive production are used to calculate the production cross sections. The list of particles is corrected at the end of each event to change the type of particles from the initial state electrons to hadrons and from the exchanged photons to Pomerons/Reggeons, or gluons, depending on the process.

The output of the FPMC generator was interfaced with the fast simulation of the ATLAS detector in the standalone ATLFAST++ package for ROOT [25]. The fast simulation of ATLAS is performed for all signal and background processes.

IV. SELECTION OF DIFFRACTIVE AND PHOTON EXCHANGE EVENTS AT HIGH LUMINOSITY AT THE LHC

In this section, we detail briefly the methods used to select diffractive and two-photon exchange events at the LHC in the ATLAS detector. The same study could be made using the CMS detector, which would lead to similar results. At high instantaneous luminosity at the LHC, it is not possible to use the so-called standard rapidity gap method since up to 30 interactions—one hard interaction and many minimum bias events—occur in the same bunch crossing. The WW exclusive production overlaps with soft interactions which fill the gap devoid of any energy and the gap selection does not work any longer.

At high luminosity, the only method to select the diffractive and photon exchange events is to detect the intact protons in the final state. We thus assume the existence of forward proton detectors in the ATLAS (or CMS) detectors. A project called AFP (ATLAS Forward Physics) is under evaluation in the ATLAS collaboration and corresponds to the installation of forward detectors at 220 and 420 m allowing to detect intact protons in the final state [26]. The acceptance of such detectors is about $0.0015 < \xi < 0.15$ where ξ is the proton momentum fraction carried by the Pomeron or the photon, and spans up to several GeV^2 in the momentum transfer $|t|$.

V. MEASURING THE $pp \to pWWp$ PROCESS IN THE STANDARD MODEL

Before discussing the possibility of observing anomalous couplings, we will mention how to discover the SM $pWWp$ process at the LHC.

A. The $pp \to pWWp$ signal

The total cross section of the exclusive process $pp \to pWWp$ where the interaction proceeds through the exchange of two quasireal photons shown in Fig. 9 is 95.6 fb and this value has to be corrected for the survival probability factor 0.9.

The cross section is rather modest in comparison to the inelastic production which is about 3 orders of magnitude higher (at $\sqrt{s} = 14$ TeV, the next-to-leading order W^+W^- cross section is 111.6 pb, produced via quark-anti-quark annihilation $q\bar{q} \to W^+W^-$ ($\sim 95\%$) and also via gluon-gluon fusion $gg \to W^+W^-$ ($\sim 5\%$). A substantial amount of luminosity has to be therefore collected to have a significant WW sample. It can only be accumulated when running at high LHC instantaneous luminosities $\mathcal{L} = 10^{33}$–10^{34} $\mathrm{cm}^{-2}\,\mathrm{s}^{-1}$. Under such running conditions, the two-photon events must be selected with the forward proton tagging detectors.

The W boson decays hadronically ($\sim 68\%$) or leptonically ($\sim 32\%$). The hadronic or semileptonic decays in which at least one jet is present could be mimicked by the

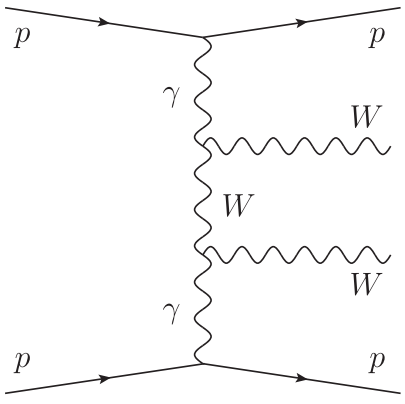

FIG. 9. Diboson production through the two-photon exchange. Intact protons leave the interaction scattered at small angles $\lesssim 100$ μrad.

QCD dijets or nondiffractive WW production, overlaid with other minimum bias interactions leading to a proton hit in the forward detectors. For simplicity, we focus on the W decays only into electrons or muons in the final state. This in turn means that also only the leptonic decays of the τ lepton ($\sim 35\%$) are considered. Semileptonic decays of the Ws will be considered in a further study. About $\sim 6\%$ of the total WW cross section is retained for the analysis. About 1800 events are produced with two leptons in the final states for 30 fb^{-1}, an integrated luminosity which corresponds approximately to the 3 first years of running. We will see further that taking into account the forward detector acceptance, and the electron/muon reconstruction efficiencies, the expected number of events drops down to 50 events.

B. Diffractive and $\gamma\gamma$ dilepton background

The clean two-leptonic signature of the two boson signal process $\gamma\gamma \to W^+W^- \to l\bar{l}\nu\bar{\nu}$ can be mimicked by several background processes which all have two intact protons in the final state. They are the following:

(1) $\gamma\gamma \to l\bar{l}$—two-photon dilepton production
(2) DPE $\to l\bar{l}$—dilepton production through double Pomeron exchange
(3) DPE $\to W^+W^- \to l\bar{l}\nu\bar{\nu}$—production of diboson through double Pomeron exchange

The double Pomeron exchange (DPE) production of dileptons and dibosons is described within the factorized Ingelman-Schlein model where the hard diffractive scattering is interpreted in terms of the colorless Pomeron with a partonic structure. Cross sections are obtained as a convolution of the hard matrix elements with the diffractive parton density functions measured at HERA [22]. Dileptons in DPE are produced as Drell-Yan pairs, probing the quark structure of the Pomerons. The exchange is carried out through γ^* or Z^*. Contrary to the two-photon exclusive case where only scattered protons and leptons in the central detector are present, in DPE events, Pomeron remnants accompany the interacting partons. They give a significant boost to the lepton pair in the transverse plane resulting in a non-negligible azimuthal decorrelation $\Delta\phi$ between the leptons. Finally, the diboson production in DPE is very similar to the actual $\gamma\gamma \to WW$ signal except that the mass distribution of the WW system is not as strongly peaked toward small values. The DPE dilepton and diboson total production cross sections at generator level are, respectively, 743 pb (all lepton families) and 211 fb (all decay modes).

The mentioned cross sections have to be multiplied by the survival probability factors (0.9 and 0.03 for two-photon and DPE processes, respectively) yielding cross sections of the signal and background shown in Table I. The dilepton production is the largest background, 3 orders of magnitude higher than the desired $\gamma\gamma \to WW$ signal.

The characteristic properties of the two-photon and DPE productions are visible in Fig. 10. The leptons (e/μ) are required to be within the generic central detector acceptance $p_T^{\mathrm{lep}1,2} > 10$ GeV, $|\eta^{\mathrm{lep}}| < 2.5$. The p_T distributions (left) are peaked toward 0. Since the leptons are predominantly produced at central pseudorapidity this reflects the steepness of the two-photon luminosity dependence as a function of $W_{\gamma\gamma}$. In the DPE dilepton spectrum one can identify the Z^* resonance around $p_T^{\mathrm{lep}1} = 45$ GeV. The diboson spectrum on the other hand slowly increases until the WW channel is totally kinematically opened and then decreases due to the drop of the effective photon-photon or Pomeron-Pomeron luminosity. On the right side of Fig. 10, the momentum fraction loss ξ distribution shows again that the two-photon production is dominant at low mass. The momentum fraction tail of the DPE is truncated at $\xi = 0.2$ which is about the limit of the validity of the factorized Pomeron model. The acceptance of the AFP detectors is shown as well. It provides us an access of two-photon masses up to $\sqrt{s} \times \xi_{\max} = 14$ TeV $\times 0.15 = 2.1$ TeV.

TABLE I. Total cross sections for SM $\gamma\gamma \to WW$ signal and background processes at 14 TeV including the gap survival probability factor (0.9 for QED and 0.03 for DPE processes). The maximal fractional momentum loss for DPE is $\xi_{\max} = 0.2$.

Process	Total cross section
$\gamma\gamma \to WW$	86 fb
$\gamma\gamma \to ll$ ($p_T^{\mathrm{lep}1} > 5$ GeV)	36 pb
DPE $\to ll$	7.4 pb
DPE $\to WW$	6.2 fb

The most natural distinction of the diboson signal is the missing transverse energy ($\not{E}_T$) in the event due to the undetected two neutrinos, see Fig. 11 (left). It provides a very effective suppression not only of the two-photon dileptons where leptons are produced back-to-back in the central detector with no intrinsic $\not{E}_T$, but suppresses also the DPE dilepton background, because some of the energy due to the Pomeron remnants is not seen in the calorimeter. It can be due to either a limited η coverage of the calorimeter or due to a minimum energy readout threshold in the system which the Pomeron remnants do not pass. Both cases mimic $\not{E}_T$.

Another way to distinguish the diboson signal is to use the missing mass $W = \sqrt{s\xi_1\xi_2}$ reconstructed in forward detectors which is shown in Fig. 11 (right). The dilepton production is dominant at low mass in both two-photon and DPE exchanges, but has also a non-negligible contribution at high mass. The azimuthal angle $\Delta\phi$ between the two leading leptons is depicted in Fig. 12. Dilepton events are more back-to-back than the diboson ones.

As mentioned before, all signal and background processes are generated using FPMC, interfaced with the fast simulation of the ATLAS detector in the standalone ATLFAST++ package. The aim was to examine the general properties of all backgrounds in a fast way to define strategies for early data measurements with the emphasis

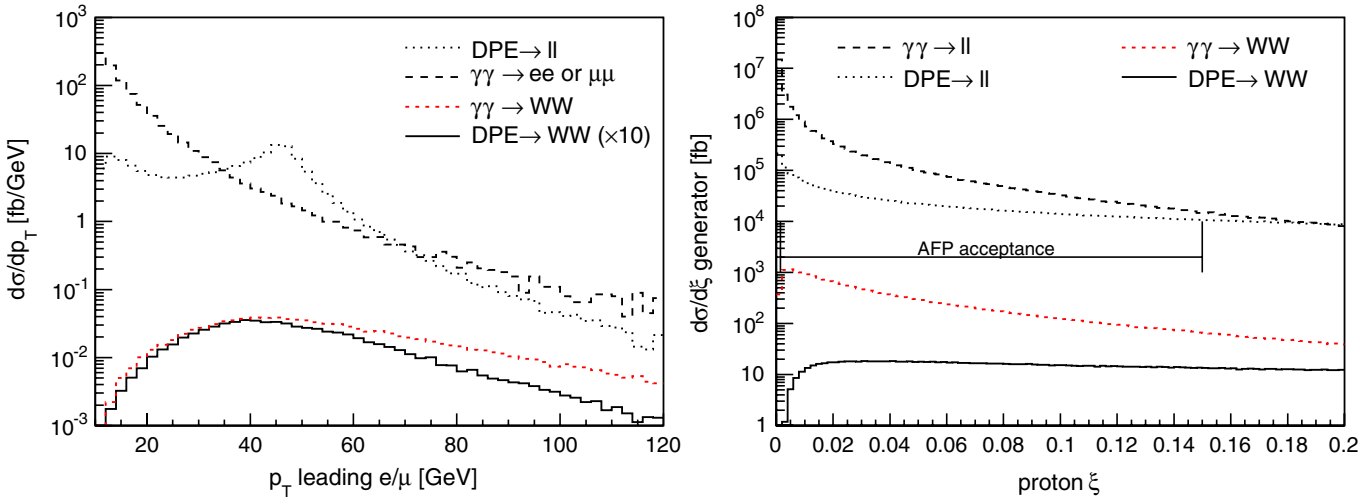

FIG. 10 (color online). Transverse momentum of the leading e or μ (left) and the momentum fraction loss ξ (right) distributions for processes which have two leptons as well as two forward intact protons in the final state. The signal $\gamma\gamma \to WW$ is outraged by the ll two-photon and DPE production.

on the two-photon dilepton and anomalous coupling studies. Effects of the charge or jet misidentifications cannot be considered in this study using a fast simulation of the ATLAS detector but will be evaluated with real data.

We will now discuss how to select the signal $\gamma\gamma \to WW$ events from the mentioned background.

C. Strategy to measure the $pp \to pWWp$ process

It is necessary to use forward detectors to search for $pp \to pWWp$ production at high luminosity. After tagging the protons with a momentum fraction $0.0015 < \xi_{1,2} < 0.15$, the signal is selected with $\not{E}_T > 20$ GeV measured in the central detector and a missing mass $W > 2m_W$ measured in forward proton detectors. Both cuts are natural for diboson production. The $\gamma\gamma \to ll$ production where leptons are produced back-to-back is completely removed requesting the azimuthal angle between the two observed leptons $\Delta\phi < 2.7$ rad.

Let us note in addition that triggering on those events is quite easy since we have two Ws in the central ATLAS detector decaying into leptons. The trigger menus of ATLAS are designed in a way to have the least possible prescales on leptons produced in electroweak bosons W/Z decays. The L1 and high level triggers can be operated without prescales up to luminosities $\mathcal{L} = 2 \times 10^{33}\ \mathrm{cm}^{-2}\,\mathrm{s}^{-1}$ with thresholds of 20 GeV for single muons, and 18 GeV at L1 and 22 GeV at the high level triggers for single electrons [27]. For higher luminosities, the trigger menus will have to be studied and tuned. In

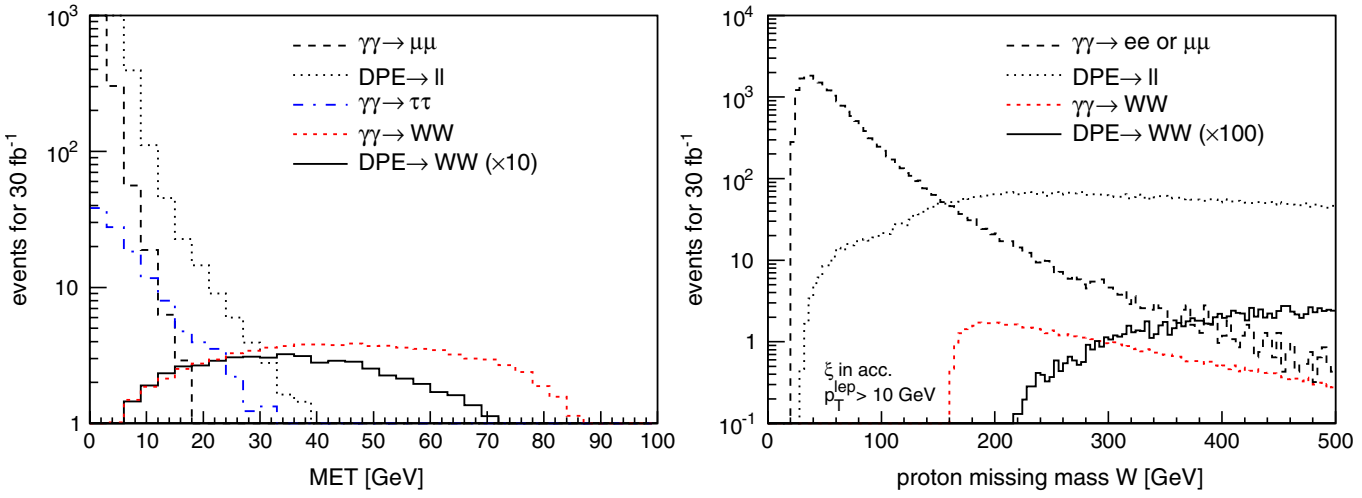

FIG. 11 (color online). Missing transverse $\not{E}_T$ energy (left) and reconstructed W missing mass in the forward detectors (right) for the two-photon WW signal and background processes. The WW signal has a production threshold at $2m_W$ and has a large $\not{E}_T$ due to the undetected neutrinos.

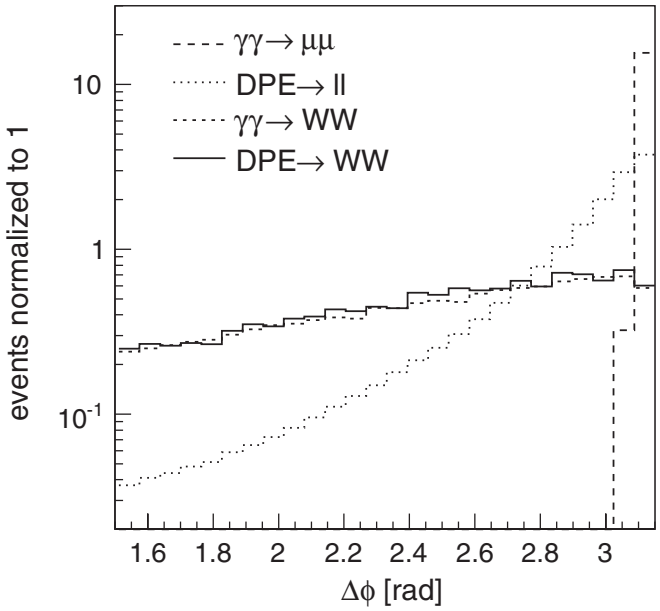

FIG. 12. $\Delta\phi$ between two leading leptons. Dilepton events are more back-to-back than diboson events. DPE dileptons is less peaked because of the presence of the Pomeron remnants which give a transverse boost to the Drell-Yan system.

addition, most of the protons will be detected in the forward proton detectors located at 220 m which can give an additional L1 trigger.

The remaining background is composed of the DPE $\rightarrow$ ll ($\sim 80\%$) and DPE $\rightarrow$ WW (20%). We handle it by requesting the transverse momentum of the leading lepton $p_T^{\mathrm{lep1}} > 25$ GeV and the missing mass smaller than $W < 500$ GeV, see Fig. 13. This leaves us with the cross section 1.69 ± 0.01 fb for the signal (the shown uncertainty reflects the statistical uncertainty of the calculation). In summary, the following requirements are used:

$$\begin{aligned} p_T^{\mathrm{lep1}} &> 25\ \mathrm{GeV}, \qquad p_T^{\mathrm{lep2}} > 10\ \mathrm{GeV}, \\ 0.0015 < \xi &< 0.15, \qquad \not{E}_T > 20\ \mathrm{GeV}, \\ 160 < W &< 500\ \mathrm{GeV}, \qquad \Delta\phi < 2.7\ \mathrm{rad}. \end{aligned} \tag{29}$$

The successive effects of all mentioned constraints are given in Table II where the number of events is shown for 30 fb^{-1}. In three years, one expects about 50.8 ± 0.2 signal events and 1.7 ± 0.1 background events. It is interesting to notice that this measurement can be successfully carried out even if the AFP acceptance does not reach its design maximum acceptance range $\xi_{\mathrm{max}} = 0.15$. The number of expected events for $\xi_{\mathrm{max}} = 0.1$, and $\xi_{\mathrm{max}} = 0.05$ are 47 ± 0.2, 32 ± 0.2 for 30 fb^{-1}. The corresponding total backgrounds are 1.4 ± 0.1 and 0.65 ± 0.08 events, respectively.

D. Results

The 5σ discovery of the $pp \rightarrow pWWp$ process could be achieved with about 5 fb^{-1} of data in the leptonic mode only. The signal significance is calculated as the P value α, i.e. as the probability to find the number of observed events or more from the background alone. For 5 fb^{-1}, the confidence $1 - \alpha$ expressed in the number of standard deviations for the Gaussian distribution reads 5.3, 5.8, 6.2 for $\xi_{\mathrm{max}} = 0.15, 0.1, 0.05$, respectively. The number of signal and background events for 5 fb^{-1} and 10 fb^{-1} together with the value of the confidence level, is given in Table III.

It should be noted that the process $pp \rightarrow pWWp$ can be discovered even with lower luminosity if one takes the full-leptonic and semileptonic decays of the two final states W into account. In [17] we considered a simplified analysis studying the two-photon WW production and the

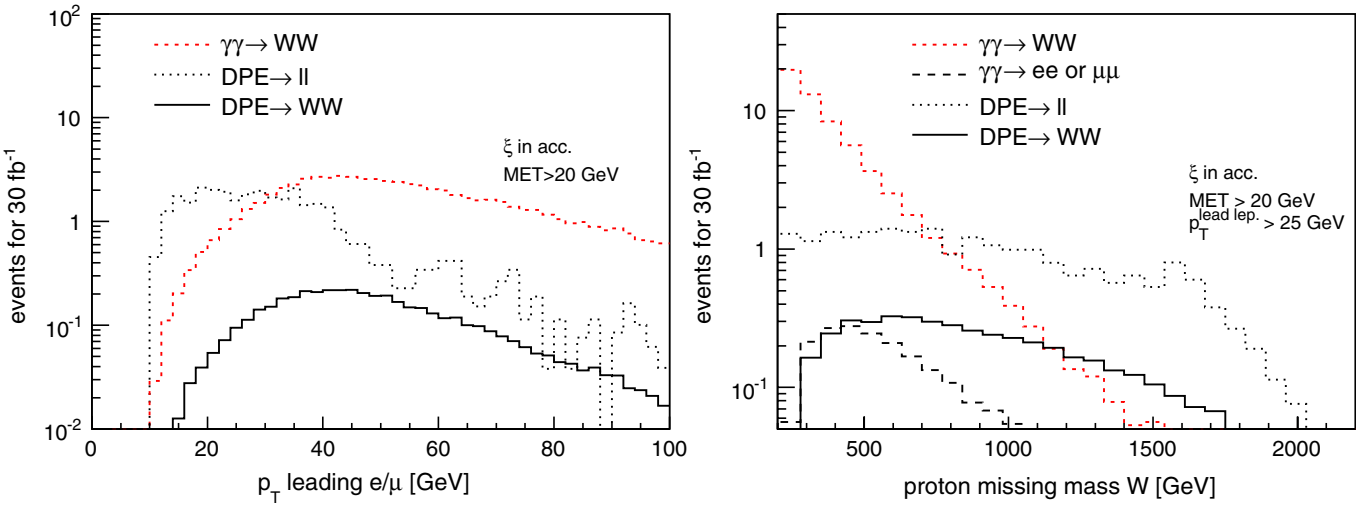

FIG. 13 (color online). Signal $\gamma\gamma \rightarrow WW$ and background before the cut on the leading lepton transverse momentum $p_T > 25$ GeV (left) and before the cut on the missing mass $W < 500$ GeV (right). Both constraints are aimed to suppress the DPE $\rightarrow$ ll production which is the most important background for the measurement.

TABLE II. Background rejection to select $\gamma\gamma \to WW$ events for $\mathcal{L} = 30$ fb^{-1}. The overall final signal is 51, 47, 32 signal events for the upper limit of the forward detector acceptance $\xi_{\max} = 0.15$, 0.1, and 0.05, respectively, whereas the background is as low as 1.7, 1.4, 0.65 events. The statistical uncertainty on the expected number of events is at most 15% and is the largest for DPE $\to ll$.

Cut/process	$\gamma\gamma \to ee$	$\gamma\gamma \to \mu\mu$	$\gamma\gamma \to \tau\tau$	DPE $\to ll$	DPE $\to WW$	$\gamma\gamma \to WW$
Gen. $p_T^{\text{lep1}} > 5$ GeV	364 500	364 500	337 500	295 200	530	1198
$p_T^{\text{lep1,2}} > 10$ GeV	24 896	25 547	177	17 931	8.8	95
$0.0015 < \xi < 0.15$	10 398	10 535	126	11 487	5.9	89
$\not{E}_T > 20$ GeV	0	0.86	14	33	4.7	78
$W > 160$ GeV	0	0.86	8.3	33	4.7	78
$\Delta\phi < 2.7$ rad	0	0	0	14	3.8	61
$p_T^{\text{lep}} > 25$ GeV	0	0	0	7.5	3.5	58
$W < 500$	0	0	0	1.0	0.67	51
$\xi < 0.1$	0	0	0	0.85	0.54	47
$\xi < 0.05$	0	0	0	0.40	0.25	32

TABLE III. Signal and total background cross sections for $\gamma\gamma \to WW$, and the $S/\sqrt{B+1}$ ratio for luminosities 5 and 10 fb^{-1} as a function of the forward detector acceptance $0.0015 < \xi < \xi_{\max}$ after all cuts mentioned in the text.

$\xi_{\max}$	Signal [fb]	Background [fb]	$S/\sqrt{B+1}$	$\mathcal{L} = 5$ fb^{-1}	$\mathcal{L} = 10$ fb^{-1}
0.05	1.69	0.06		7.5	14
0.1	1.57	0.05		7.1	13
0.15	1.07	0.02		5.1	9.1

DPE $\to WW$ background only assuming that the overlaid background due to multiple interactions is removed with timing detectors. Events with at least one lepton above $p_T^{\text{lep1}} > 30$ GeV in addition to both proton tags in forward detectors $0.0015 < \xi_{1,2} < 0.15$ were selected. The full-hadronic W decays were rejected in order to remove the high QCD dijet background. It turned out that the process can be discovered already with 400 pb^{-1} of integrated luminosity by observing 11 signal events and 0.9 background yielding a confidence 5.8. The higher sensitivity to the two-photon WW production is of course due to the higher cross section when one takes into account the semileptonic decays. In this case, however, a new background arises from the central exclusive production of two quarks which was not studied. If one of the quarks radiates a W boson, the W + jet + jet final state mimics the semileptonic WW decays in two-photon production. This background process is planned to be included in future releases of FPMC to allow a complete study of the two-photon WW production even in the semileptonic decay mode [28].

VI. SENSITIVITY TO QUARTIC ANOMALOUS COUPLING OF W AND Z TO PHOTON

A. Signal cross section for quartic couplings

In this section, we study the phenomenological consequences of the new anomalous terms in the Lagrangian. The implementation in the FPMC generator allowed us to compare the studied signal due to anomalous couplings directly with all backgrounds that leave the proton intact and create two leptons, electrons or muons, in the central detector.

As shown in Fig. 4, we recall that the anomalous couplings in $pp \to pWWp$ and $pp \to pZZp$ processes augment the cross section from their SM values 95.6 fb and 0. The suppression of the cross section due to the form factors is shown in Fig. 5. It is important to stress that this effect is large and it has to be taken into account when deriving the sensitivities to the anomalous couplings.

B. Background rejection at high luminosity for WW signal

In Fig. 14, the p_T distributions of the signal due to quartic couplings and the background are superimposed. As expected, the signal due to anomalous coupling appears at high transverse momentum, or at high masses. The first cut used in the analysis is therefore to select high p_T leptons together with intact protons in the final state detected in the forward detectors to identify the exclusive two-photon events. At high luminosity, the forward detector acceptance (high cut on $\xi < 0.15$) removes the highest mass events and part of the signal due to anomalous coupling which appears at high masses is not observed.

The WW events which give a hit in both forward detectors are first selected with $\not{E}_T > 20$ GeV. The $\not{E}_T$ dependence is depicted in Fig. 15 (left) for the signal $a_0^W/\Lambda^2 = 2 \times 10^{-6}$ GeV^{-2} and the background. Note that the signal is barely distinguishable from the SM

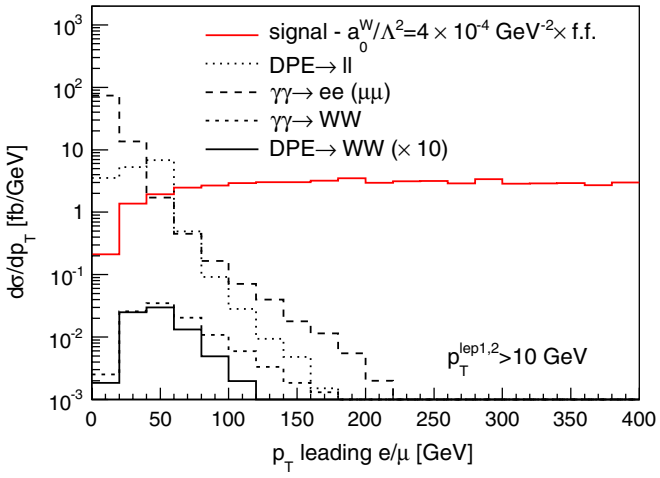

FIG. 14 (color online). Contribution of various background processes to the signal with anomalous coupling $a_0^W/\Lambda^2 = 3 \times 10^{-4}$ GeV^{-2} with the coupling form factors taken into account at generator level. The signal due to the anomalous coupling manifest itself at high transverse lepton momenta.

$\gamma\gamma \to WW$ process. On the other hand, processes in which lepton pairs are created directly through $\gamma\gamma$ or DPE exchange are greatly suppressed. The next cut focuses on the high diphoton mass $W_{\gamma\gamma}$ where the signal is preferably enhanced. In Fig. 15 (right) we see that the signal due to anomalous coupling is well selected if the reconstructed missing mass in the forward detectors is $W > 800$ GeV. It was verified that such selection applies for all anomalous parameters in question in a very similar way, i.e. that the $W > 800$ GeV retains the interesting signal for a wide range of anomalous parameters.

The most dominant background which remains is the DPE $\to ll$ production. A large part of this background is removed by requesting the angle between reconstructed leptons $\Delta\phi < 3.13$ rad as illustrated in Fig. 16 (left). This removes also the potential two-photon dileptons. However, the $\Delta\phi$ cut cannot be arbitrarily relaxed because we would remove part of the signal also. We also require the dilepton mass to be far from the Z pole in order to reduce the DPE $\to ll$ production.

To summarize, the following cuts are used to select the anomalous signal at high luminosity

$$\begin{aligned} p_T^{\text{lep1}} &> 160 \text{ GeV}, & p_T^{\text{lep2}} &> 10 \text{ GeV}, \\ 0.0015 < \xi &< 0.15, & \not{E}_T &> 20 \text{ GeV}, \\ W &> 800 \text{ GeV}, & M_{ll} &\notin \langle 80, 100 \rangle \text{ GeV}, \\ \Delta\phi &< 3.13 \text{ rad}. \end{aligned} \tag{30}$$

Finally, the p_T^{lep} distribution after all mentioned constrains is shown in Fig. 16 (right). The remaining background is composed not only from the expected $\gamma\gamma \to WW$ production but also from DPE $\to ll$ by about an equal amount.

The successive effect of all cuts and their rejection power of the background is summarized in Table IV where the number of events is shown for $\mathcal{L} = 30$ fb^{-1}. The total number of background events is thus reduced to 0.90 ± 0.05.The effect of these cuts for the signals $|a_0^W/\Lambda^2| = 5.4 \cdot 10^{-6}$ GeV^{-2} and $|a_C^W/\Lambda^2| = 20 \cdot 10^{-6}$ GeV^{-2} all shown in Table V.

C. Background rejection at high luminosity for the ZZ signal

The Z pair production is background free in the leading order provided that the nondiffractive background is removed using the forward detectors tagging the intact protons. The complete set of used cuts is

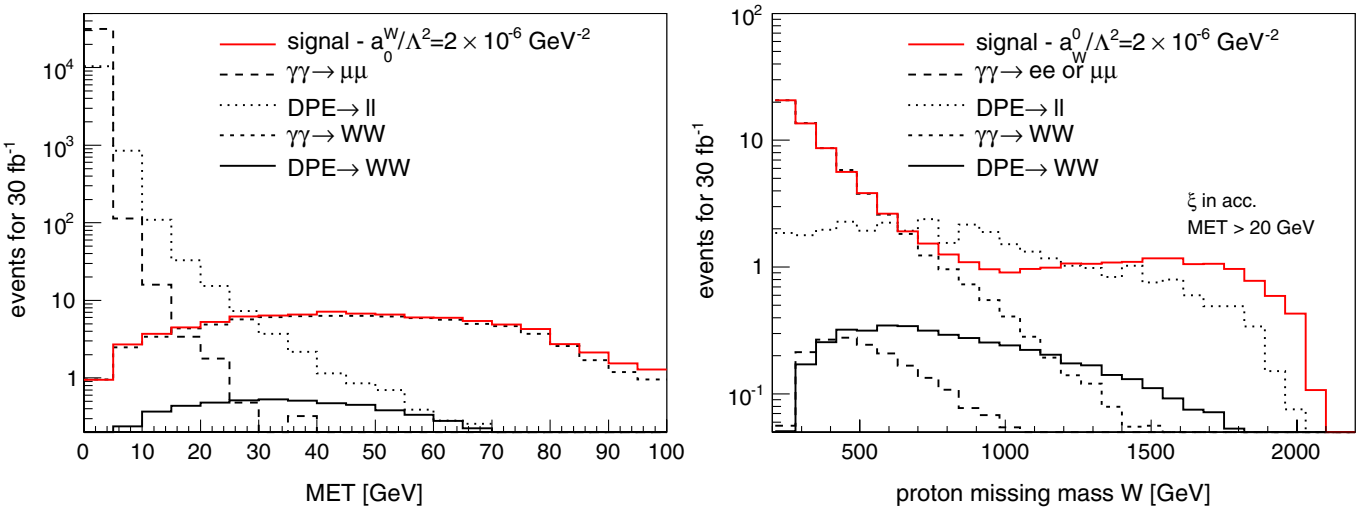

FIG. 15 (color online). Missing transverse energy distribution $\not{E}_T$ in the AFP detector acceptance cut (left) and proton missing mass (right) in the AFP acceptance and after the cut on $\not{E}_T > 20$ GeV cut for signal and all backgrounds with $\mathcal{L} = 30$ fb^{-1}.

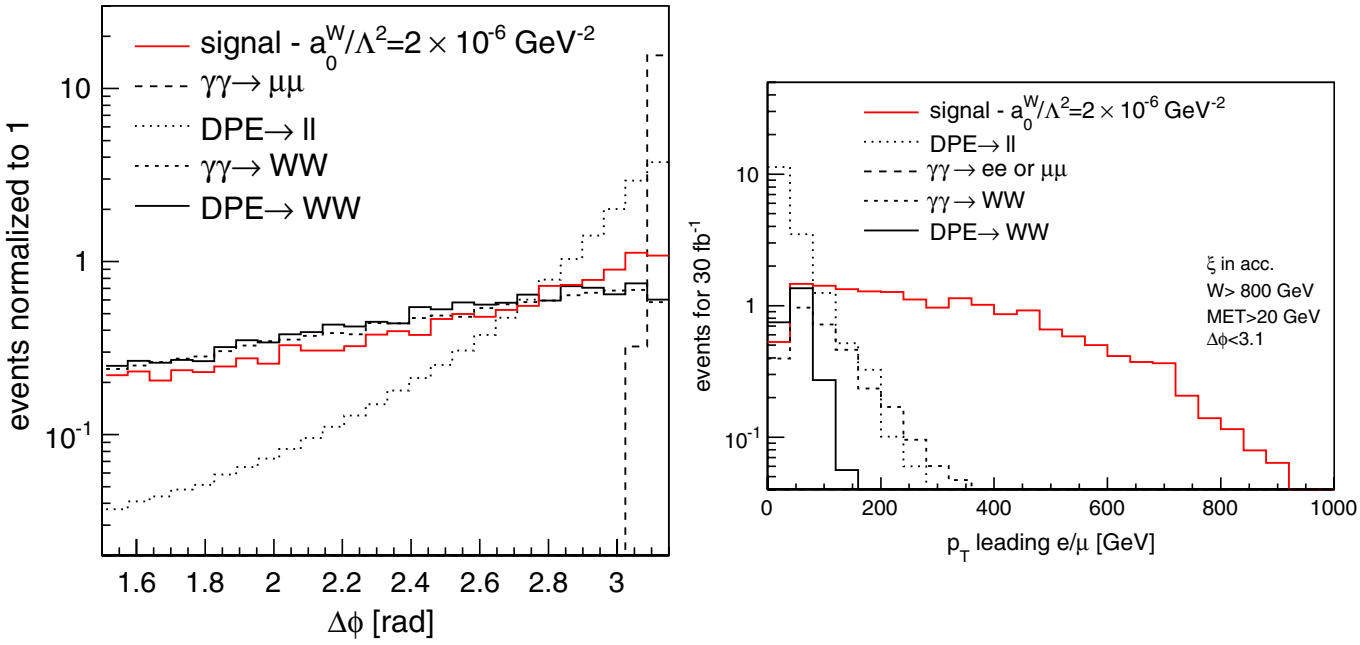

FIG. 16 (color online). Angle between detected leptons (left) and p_T distribution of the leading lepton (right) after all cuts as mentioned in the text for signal and background. The events are normalized for $\mathcal{L} = 30$ fb^{-1}.

TABLE IV. Rejection of the background by successive application of the selection cuts. The number of events is normalized to $\mathcal{L} = 30$ fb^{-1} of integrated luminosity. The lepton index lep corresponds to electrons or muons. The DPE $\rightarrow ll$ was generated with a minimum Drell-Yan mass 10 GeV. The largest statistical uncertainty is 7% for DPE $\rightarrow ll$ after all cuts.

	Events for 30 fb^{-1}					
Cut/process	$\gamma\gamma \rightarrow ee$	$\gamma\gamma \rightarrow \mu\mu$	$\gamma\gamma \rightarrow \tau\tau$	$\gamma\gamma \rightarrow WW$	DPE $\rightarrow ll$	DPE $\rightarrow WW$
gen. $p_T^{\text{lep1}} > 5$ GeV	364 500	364 500	337 500	1198	295 200	530
$p_T^{\text{lep1,2}} > 10$ GeV	24 895	25 547	177	99	18 464	8.8
$0.0015 < \xi < 0.15$	10 398	10 534	126	89	11 712	6.0
$\not{E}_T > 20$ GeV	0	0.86	14	77	36	4.7
$W > 800$ GeV	0	0.27	0.15	3.2	16	2.5
$M_{ll} \notin \langle 80, 100\rangle$	0	0.27	0.15	3.2	13	2.5
$\Delta\phi < 3.13$ rad	0	0	0.10	3.2	12	2.5
$p_T^{\text{lep1}} > 160$ GeV	0	0	0	0.69	0.20	0.024

TABLE V. Selection of the signal by successive application of the cuts. The number of events is given for integrated luminosity of $\mathcal{L} = 30$ fb^{-1}. The lepton index lep corresponds to electrons or muons.

	Events for 30 fb^{-1}	
Cut/couplings (with f.f.)	$\lvert a_0^W/\Lambda^2\rvert = 5.4 \cdot 10^{-6}$ GeV^{-2}	$\lvert a_C^W/\Lambda^2\rvert = 20 \cdot 10^{-6}$ GeV^{-2}
$p_T^{\text{lep1,2}} > 10$ GeV	202	200
$0.0015 < \xi < 0.15$	116	119
$\not{E}_T > 20$ GeV	104	107
$W > 800$ GeV	24	23
$M_{ll} \notin \langle 80, 100\rangle$	24	23
$\Delta\phi < 3.13$ rad	24	22
$p_T^{\text{lep1}} > 160$ GeV	17	16

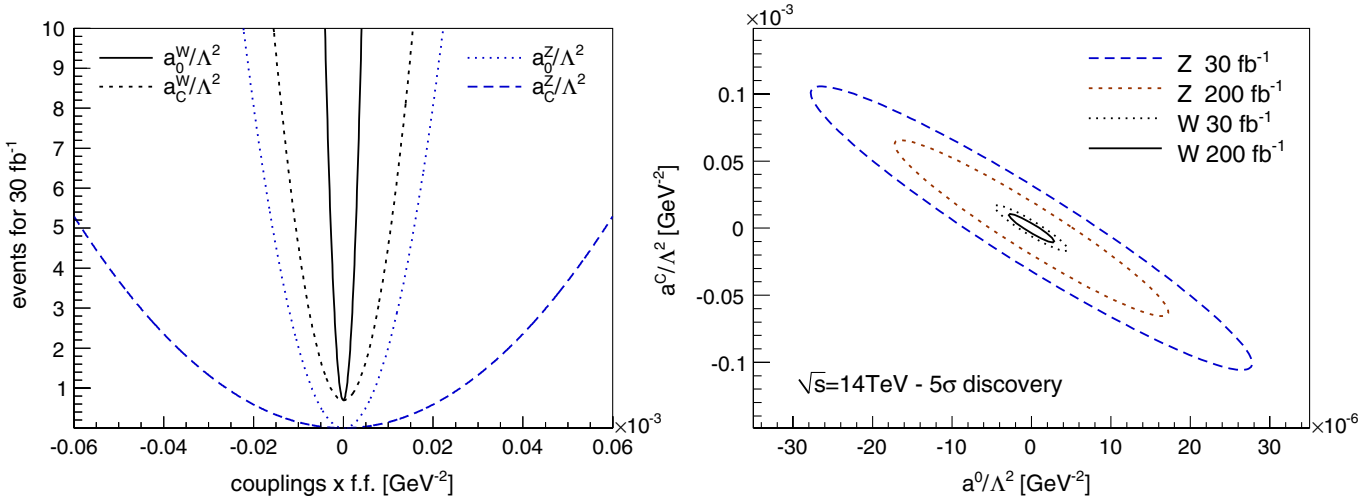

FIG. 17 (color online). Number of events for signal (left) due to different values of anomalous couplings after all cuts (see text) for $\mathcal{L} = 30$ fb^{-1}, and 5σ discovery contours (right) for all the WW and ZZ quartic couplings at $\sqrt{s} = 14$ TeV for $\mathcal{L} = 30$ fb^{-1} and $\mathcal{L} = 200$ fb^{-1}.

$$[(n_{\mathrm{lep}} \geq 2, 2 \text{ of same charge}) \quad \text{or} \quad n_{\mathrm{lep}} \geq 3],$$
$$0.0015 < \xi < 0.15, \qquad p_T^{\mathrm{lep1}} > 160 \text{ GeV}, \tag{31}$$
$$p_T^{\mathrm{lep2}} > 25 \text{ GeV}.$$

D. Sensitivity at high luminosity

The number of events after all cuts as a function of the anomalous parameters shown in Fig. 17 (left) is used to calculate the exclusion upper limits. The results are summarized in Tables VI and VII for $\mathcal{L} = 30$ fb^{-1} and $\mathcal{L} = 200$ fb^{-1}, respectively.

TABLE VI. 95% C.L. interval, 3σ evidence, and 5σ discovery potential on the $WW\gamma\gamma$ and $ZZ\gamma\gamma$ anomalous quartic parameters using $\mathcal{L} = 30$ fb^{-1} of data at high luminosity with forward detectors, and with or without the form factors applied.

		Limits [10^{-6} GeV^{-2}]			
	Form factor	$\lvert a_0^W/\Lambda^2\rvert$	$\lvert a_C^W/\Lambda^2\rvert$	$\lvert a_0^Z/\Lambda^2\rvert$	$\lvert a_C^Z/\Lambda^2\rvert$
95% C.L.	$\Lambda_{\mathrm{cut}} = \infty$	1.2	4.2	2.8	10
	$\Lambda_{\mathrm{cut}} = 2$ TeV	2.6	9.4	6.4	24
3σ evidence	$\Lambda_{\mathrm{cut}} = \infty$	1.6	5.8	4.0	14
	$\Lambda_{\mathrm{cut}} = 2$ TeV	3.6	13	9.0	34
5σ discovery	$\Lambda_{\mathrm{cut}} = \infty$	2.3	9.7	6.2	23
	$\Lambda_{\mathrm{cut}} = 2$ TeV	5.4	20	14	52

TABLE VII. 95% C.L. interval, 3σ evidence, and 5σ discovery potential on the $WW\gamma\gamma$ and $ZZ\gamma\gamma$ anomalous quartic parameters using $\mathcal{L} = 200$ fb^{-1} of data at high luminosity with forward detectors, and with or without the form factors applied. 95% C.L. limit, 3σ evidence, and 5σ discovery potential correspond to the values of the couplings outside of the quoted intervals.

		Limits [10^{-6} GeV^{-2}]			
	Form factor	$\lvert a_0^W/\Lambda^2\rvert$	$\lvert a_C^W/\Lambda^2\rvert$	$\lvert a_0^Z/\Lambda^2\rvert$	$\lvert a_C^Z/\Lambda^2\rvert$
95% C.L.	$\Lambda_{\mathrm{cut}} = \infty$	0.7	2.4	1.1	4.1
	$\Lambda_{\mathrm{cut}} = 2$ TeV	1.4	5.2	2.5	9.2
3σ evidence	$\Lambda_{\mathrm{cut}} = \infty$	0.85	3.0	1.6	5.7
	$\Lambda_{\mathrm{cut}} = 2$ TeV	1.8	6.7	3.5	13
5σ discovery	$\Lambda_{\mathrm{cut}} = \infty$	1.2	4.3	4.1	8.9
	$\Lambda_{\mathrm{cut}} = 2$ TeV	2.7	9.6	5.5	20

TABLE VIII. Selection of the $\Delta\kappa^\gamma$ and λ^γ signal by the successive application of the cuts. The number of events is given for integrated luminosity $\mathcal{L} = 30$ fb^{-1}.

Events for 30 fb^{-1} Cut	$\Delta\kappa^\gamma = 0.3$ (with f.f.)
$p_T^{\text{lep1,2}} > 10$ GeV	194
$0.0015 < \xi < 0.15$	179
$\not{E}_T > 20$ GeV	158
$W > 160$ GeV	158
$\Delta\phi < 2.7$ rad	118
$p_T^{\text{lep1}} > 25$ GeV	112
$W < 500$	98

Events for 30 fb^{-1} cut	$\lambda^\gamma = 0.1$ (with f.f.)
$p_T^{\text{lep1,2}} > 10$ GeV	168.
$0.0015 < \xi < 0.15$	119
$\not{E}_T > 20$ GeV	107
$W > 800$ GeV	25
$M_{ll} \notin \langle 80, 100\rangle$	25
$\Delta\phi < 3.13$ rad	24
$p_T^{\text{lep1}} > 160$ GeV	19

Comparing our results with the OPAL limits (18) we see that the improvement of sensitivities which can be obtained with a collected luminosity 30 fb^{-1} corresponding approximately to three years of running with the forward detectors, is about a factor of 5000 for all couplings except a_C^Z/Λ^2 where the improvement is about a factor 5 worse. With the full $\mathcal{L} = 200$ fb^{-1} luminosity, the improvement reaches about a factor of 10 000. When two of the anomalous parameters are varied independently, the sensitivities form an ellipse in $a_C/\Lambda^2 \times a_0/\Lambda^2$ plane as shown in Fig. 17 (right).

VII. SENSITIVITY TO ANOMALOUS TRIPLE GAUGE $WW\gamma$ COUPLING AT HIGH LUMINOSITY

A. Signal selection

The limits on triple gauge boson anomalous couplings obtained at LEP and the Tevatron are already very stringent, more than in the case of quartic anomalous couplings. Let us however remind that triple and genuine quartic anomalous couplings are not related in any way. Hence, the analysis which has been performed above for the quartic couplings has its own importance irrespective of the triple ones. The production cross sections corresponding to the current limits for $\Delta\kappa^\gamma$ and λ^γ are rather small, hence, the only option to gain an improvement is again to consider the high luminosity scenario with forward detectors.

The signal selection follows closely two already defined strategies. Since $\Delta\kappa^\gamma$ changes only the normalization, the signal at low W masses has to be retained. Therefore the selection of the signal is the same as it was optimized for the measurement of the SM $pp \to pWWp$ cross section (Sec. V C). On the contrary, the signal due to λ^γ parameters appears at high mass with high p_T objects created in the central detector. We can simply use the signal selection requirements designed for the quartic couplings discussed in (Sec. VI B). For clarity, we use the following cuts for $\Delta\kappa^\gamma$:

$$\begin{aligned} &p_T^{\text{lep1}} > 25 \text{ GeV}, \quad p_T^{\text{lep2}} > 10 \text{ GeV}, \\ &0.0015 < \xi < 0.15, \quad \not{E}_T > 20 \text{ GeV}, \\ &160 < W < 500 \text{ GeV}, \quad \Delta\phi < 2.7 \text{ rad} \end{aligned} \tag{32}$$

and for λ^γ

$$\begin{aligned} &p_T^{\text{lep1}} > 160 \text{ GeV}, \quad p_T^{\text{lep2}} > 10 \text{ GeV}, \\ &0.0015 < \xi < 0.15, \quad \not{E}_T > 20 \text{ GeV}, \\ &W > 800 \text{ GeV}, \quad M_{ll} \notin \langle 80, 100\rangle \text{ GeV}, \\ &\Delta\phi < 3.13 \text{ rad}. \end{aligned} \tag{33}$$

The expected backgrounds for $\mathcal{L} = 30$ fb^{-1} are 1.7 ± 0.1 for $\Delta\kappa^\gamma$ and 0.90 ± 0.05 for λ^γ as discussed in Secs. V C and VI B. The successive application of all mentioned requirements for $\Delta\kappa^\gamma$ and λ^γ signal is detailed in Table VIII for $\mathcal{L} = 30$ fb^{-1}.

B. Sensitivities at high luminosities

The sensitivities are summarized in Table IX for 30 and 200 fb^{-1}. Comparing these values with the current limits from the Tevatron, we see that the improvement is limited, about a factor of 2 with 30 fb^{-1} of collected luminosity.

Let us also compare the results to those obtainable in the conventional ATLAS analysis without forward detectors.

TABLE IX. 95% C.L., 3σ evidence, and 5σ discovery potential on the $WW\gamma$ anomalous parameters for a luminosity of $\mathcal{L} = 30$ fb^{-1} and 200 fb^{-1} using the AFP forward detectors with coupling form factors applied.

	$\mathcal{L} = 30$ fb^{-1}		$\mathcal{L} = 200$ fb^{-1}	
	$\Delta\kappa^\gamma$	λ^γ	$\Delta\kappa^\gamma$	λ^γ
95% C.L. {	$[-0.25, 0.16]$	$[-0.052, 0.049]$	$[-0.096, 0.057]$	$[-0.023, -0.027]$
3σ evidence {	$[-0.39, 0.25]$	$[-0.066, 0.064]$	$[-0.136, 0.087]$	$[-0.037, 0.038]$
5σ evidence {	$[-0.67, 0.40]$	$[-0.088, 0.094]$	$[-0.26, 0.16]$	$[-0.053, 0.049]$

TABLE X. 95% C.L. limits on the $WW\gamma$ coupling parameters obtained from fitting the p_T^γ and $M_T(WW)$ distributions in $W\gamma$ and WW final states in inelastic production in ATLAS, and calculated for $\mathcal{L} = 30$ fb^{-1} and for the form factors $\Lambda = 2$ TeV, $n = 2$ [27].

	$\Delta\kappa^\gamma$	λ^γ
$W\gamma$, (p_T^γ)	$[-0.11, 0.05]$	$[-0.02, 0.01]$
WW, (M_T)	$[-0.056, 0.054]$	$[-0.052, 0.100]$

$WW\gamma$ anomalous couplings are probed by fitting the p_T^γ spectrum of the photon distribution to the next-to-leading order expectation using the combined sample of $W(e\nu)\gamma$ and $W(\mu\nu)\gamma$ events or by fitting the transverse mass distribution $M_T(WW)$ of the boson pair, reconstructed from the two observed leptons and the missing transverse energy [27]. The corresponding 95% C.L. limits obtained for $\mathcal{L} = 30$ fb^{-1}, with the same form factor assumption as before (24) are shown in Table X. The presented analysis using forward detectors has about a factor 2 worse precision than the analysis in nondiffractive studies and would therefore be a complementary measurement.

The disadvantage of the full-leptonic (e/μ) channel of the boson decays is the small rates since only $\approx 4\%$ of the signal is kept. In the work presented in [17], we performed a quite simple analysis (without simulating all possible backgrounds) assuming that $\gamma\gamma \to WW$ and DPE $\to WW$ are the only important backgrounds, but keeping also the semileptonic events. The improvement for λ^γ with respect to the analysis with leptonic decays is only modest, since the selection was not optimized for high masses where the signal appears. On the other hand, the larger signal sample when semileptonic decays are included yields a better separation of the signal due to the $\Delta\kappa^\gamma$ anomalous parameter with respect to the SM $\gamma\gamma \to WW$ production and the sensitivity is improved by a factor 4. However, the full study using the semileptonic decays and all simulated backgrounds will be performed in an incoming paper. Especially, we still need to implement one additional background in FPMC due to the central exclusive production of $q\bar{q}$ pairs in which one of the quarks radiates a W boson. This process has not been considered in the phenomenological studies of this kind so far.

VIII. CONCLUSION

In this paper, it was first shown how the SM two-photon production $pp \to pWWp$ process with both Ws decaying leptonically could be selected from the diffractive or exclusive background. Using the forward detectors, about 50 events can be observed with 30 fb^{-1} of collected luminosity corresponding approximately to 3 years of data taking whereas the number of background processes could be kept at a few events level. No multiple interaction background was studied, but the boson invariant mass $2 \times m_W$ threshold could be used to suppress this background using the AFP proton tagging (in addition, the proton arrival time measured with special fast timing detectors can be used to further suppress the overlap background).

The sensitivities to triple and quartic gauge anomalous couplings in W production via photon induced processes were studied using the standalone ATLFAST++ simulation. To reduce the number of background events for this first study, only leptonic decays of the Ws were considered, and the case of the semileptonic decays will be the subject of an incoming paper. Using a high luminosity of 30 or 200 fb^{-1} with the forward detectors to tag the exclusive two-photon events, the sensitivities to the quartic couplings can be improved by more than 4 orders of magnitude.

On the other hand, the improvement of the triple gauge coupling experimental constraints is smaller. In the full-leptonic channel, the $\Delta\kappa^\gamma$ analysis cannot yield better results than the current limits coming from OPAL; however, it can give better results than those from the Tevatron. On the other hand, the λ^γ parameter can be fully constrained by a factor 2 better with respect to the OPAL Collaboration at LEP.

[1] P. J. Dervan, A. Signer, W. J. Stirling, and A. Werthenbach, J. Phys. G **26** 607 (2000); W. J. Stirling and A. Werthenbach, Eur. Phys. J. C **14**, 103 (2000).

[2] O. J. P. Eboli, M. C. Gonzales-Garcia, S. M. Lietti, and S. F. Novaes, Phys. Rev. D **63**, 075008 (2001); G. Cvetič and B. Koegerler, Nucl. Phys. **B363**, 401 (1991); A. Hill and J. J. van der Bij, Phys. Rev. D **36**, 3463 (1987);

[3] J. de Favereau *et al.*, arXiv:0908.2020.

[4] M. Boonekamp, V. Juránek, O. Kepka, and C. Royon, arXiv:0903.3861; http://cern.ch/fpmc.

[5] V. M. Budnev, I. F. Ginzburg, G. V. Meledin, and V. G. Serbo, Phys. Rep. **15**, 181 (1975).

[6] M. Boonekamp, C. Royon, J. Cammin, and R. B. Peschanski, Phys. Lett. B **654**, 104 (2007).

[7] J. M. Cornwall, D. N. Levin, and G. Tiktopoulos, Phys. Rev. Lett. **30**, 1268 (1973); **31**, 572(E) (1973).

[8] J. M. Cornwall, D. N. Levin, and G. Tiktopoulos, Phys. Rev. D **10**, 1145 (1974); **11**, 972(E) (1975).

[9] A. Denner, S. Dittmaier, and R. Schuster, arXiv:hep-ph/9601355.

[10] T. Pierzchala and K. Piotrzkowski, Nucl. Phys. B, Proc. Suppl. **179**, 257 (2008).

[11] V. Khoze and M. Ryskin (private communication).

[12] C. Amsler *et al.* (Particle Data Group), Phys. Lett. B **667**, 1 (2008).

[13] G. Belanger and F. Boudjema, Phys. Lett. B **288**, 201

(1992).
[14] G. Abbiendi *et al.* (OPAL Collaboration), Phys. Rev. D **70**, 032005 (2004).
[15] O. J. P. Eboli, M. C. Gonzalez-Garcia, S. M. Lietti, and S. F. Novaes, Phys. Rev. D **63**, 075008 (2001).
[16] K. Hagiwara, R. D. Peccei, D. Zeppenfeld, and K. Hikasa, Nucl. Phys. **B282**, 253 (1987).
[17] O. Kepka and C. Royon, Phys. Rev. D **78**, 073005 (2008).
[18] J. Alcaraz *et al.* (LEP Electroweak Working Group), arXiv:hep-ex/0612034.
[19] V. M. Abazov *et al.* (D0 Collaboration), Phys. Rev. Lett. **100**, 241805 (2008).
[20] G. Marchesini *et al.*, Comput. Phys. Commun. **67**, 465 (1992).
[21] E. Boos *et al.* (CompHEP Collaboration), Nucl. Instrum. Methods Phys. Res., Sect. A **534**, 250 (2004).
[22] A. Aktas *et al.* (H1 Collaboration), Eur. Phys. J. C **48**, 715 (2006); ()**48**, 749 (2006); S. Chekanov (ZEUS Collaboration), Nucl. Phys. **B800**, 1 (2008).
[23] G. Altarelli and G. Parisi, Nucl. Phys. **B126**, 298 (1977); V. N. Gribov and L. N. Lipatov, Yad. Fiz. **15**, 438 (1972) [Sov. J. Nucl. Phys. **15**, 675 (1972)]; Yu. L. Dokshitzer, Sov. Phys. JETP **46**, 641 (1977).
[24] V. A. Khoze, A. D. Martin, and M. G. Ryskin, Eur. Phys. J. C **23**, 311 (2002); E. Gotsman, E. Levin, U. Maor, E. Naftali, and A. Prygarin, arXiv:hep-ph/0511060.
[25] ATLFAST++ package for ROOT, http://root.cern.ch/root/Atlfast.html.
[26] M. G. Albrow *et al.*, JINST **4**, T10001 (2009); C. Royon, arXiv:0706.1796.
[27] G. Aad *et al.* (ATLAS Collaboration), arXiv:0901.0512.
[28] V. Khoze and W. J. Stirling (private communication).